

Energy analysis of the daylighting from a double-pane glazed window with enclosed horizontal slats in the tropics

Andhy Muhammad Fathoni, Pipat Chaiwiwatworakul*, Vichuda Mettanant

The Joint Graduate School of Energy and Environment, CHE Center for Energy Technology and Environment, King Mongkut's University of Technology Thonburi, 126 Pracha-Uthit Road, Bangmod, Tungku, Bangkok 10140, Thailand



ARTICLE INFO

Article history:

Received 25 May 2015

Received in revised form 29 March 2016

Accepted 9 June 2016

Available online 1 July 2016

Keywords:

Daylighting

Thermal gain

Slats

Sun shading

Tropical climate

ABSTRACT

Daylighting is perceived to be a potential measure for energy conservation in commercial buildings. In Thailand where the sky is highly luminous and daytime is long throughout the year, daylighting is however neglected by the use of heat reflective glasses to prevent excessive solar gain from windows. To address the issue, this paper investigates the energy performance of the daylighting from a window with horizontal slats located between two panes of glasses (slat window). The slats can shade the intense beam radiation, but allow penetration of the diffuse daylight for interior illumination. In the study, a model was developed to determine the thermal gain from the slat window. By using the thermal model together with the daylight model developed earlier, the simulations were performed and the results show that the slat window, when used with typical office room, can save 25–70% of the total electrical energy of air-conditioning and lighting in the same room equipped with heat reflective glass window.

© 2016 Elsevier B.V. All rights reserved.

1. Introduction

Glazed windows are a critical component of building envelope that influences highly on the building energy demand. In the tropics where the sky is luminous and the daytime is long throughout the year [1–3], natural daylight from side-windows to supplement artificial light from electric lamps is energy efficient for building interior illumination [4,5].

In Thailand, large glazed windows with no external shading are a popular envelope feature for high-rise commercial buildings. To avoid the excessive solar gain from the windows, heat reflective glasses with low optical transmittance are chosen for the usage. This practice leads to the negligence of the daylight use and the loss of the connectedness between building occupants and exterior scenes. For such buildings, non-dimmable electric lamps are the sole source of the interior lighting that typically shares 20% of the total building electricity use. The dissipated heat from the lamps also contributes 20% of the building cooling load. As the air-conditioning consumes 60% of the building electrical energy, the lighting contributes indirectly another 12% of the electricity use through the air-conditioning system [6]. These figures are significant and warrant attention.

In order to study the trade-off between use of daylighting and avoidance of solar heat gains, this study examines a glazing unit integrated with horizontal shading slats located between two glass panes, called the slat window herein. The slat window is of particular interest in which the slats are versatile to regulate the daylight and heat transmission into buildings. Studies of the thermal performance of the slat window have been carried out in different locations and climates. Rheault and Bilgen [7,8] developed a model of the heat transfer through the slat window. The model was used to determine the slat angles that minimize the heating and cooling loads from the window under a typical Canadian climate. Chaiyapinunt [9,10] introduced a steady-state heat transfer model of a glazed window with slats that are treated as an effective layer of the multi-layer window system. This model accounts for thickness and curvature of slats. Kuhn [11,12] developed a model to calculate effective total solar energy transmittance for venetian blinds. The model has been applied for evaluating the performance of the façade with venetian blinds and for designing of two new sun-shading products. Alessandro et al. [13] improved the Kuhn's model [11] by dividing properties of glazing and blinds into three parts: ultraviolet, visible, and near-infrared, which leads to eliminating the need of angular glazing properties as input data but ensures accuracy of the model. Zanghirella et al. [14] presented a numerical model which was developed in the Simulink/Matlab® environment to simulate the thermal behavior of mechanically ventilated active transparent facades with different configurations such as number

* Corresponding author.

E-mail addresses: pipat.ch@jgsee.kmutt.ac.th, [\(P. Chaiwiwatworakul\).](mailto:pipat@gmail.com)

Nomenclature

S	Length of the segment on the blind slat (m)
W	Width of blind slat (m)
I	Incident radiation (W/m^2)
E	Irradiation (W/m^2)
J	Radiosity (W/m^2)
A	Absorbed energy (W/m^2)
q	Heat transfer (W/m^2)

Greek symbols

φ	Profile angle and tilt angle measured with respect to the horizontal direction (deg.)
ϕ	Zenith angle (deg.)
α	Altitude angle or elevation angle (deg.)
γ	Azimuth angle (deg.)
η	Incident angles of the sun ray on surface (deg.)
τ	Transmittance of glazing
ρ	Reflectance of surface

Subscripts

l	Associated with slat
wo	Associated with outer window
wi	Associated with inner window
b	Beam normal
d	Diffuse horizontal
g	Global horizontal
c	Convention
r	Radiation

and type of glazings, airflow rate, size of the ventilated cavity, and type of shading device. In USA, Lee et al. [15] conducted full-scale experiments to study the performance of the slat window by using two office-like rooms. The measured results showed that the slat window was capable of substantially reducing both the space cooling load and the energy for electric lighting. In Korea, Oh et al. [16] demonstrated by simulations using EnergyPlus program that a window with the slat-type blind can greatly improve the energy efficiency of buildings required both space heating and cooling, and the visual comfort of building occupants. Referred to the program manual [17], the heat transfer calculation assumes the glass layer is isothermal and has no heat storage. For the daylight calculation, the direct light from a window contributing to a point on the workplane is obtained by integrating the luminance over the window surface. The internally reflected component of the workplane daylight is determined by using either the split-flux method or the radiosity method.

Other studies conducted daylight simulations that achieved optimal solutions of window configurations and tilted angles of slats [18–20]. Alzoubi [21] employed a light simulation software named Lightscape to investigate the daylight distribution in a typical small office whose window was equipped with slats. The study cautioned on excessive daylight on the area next to the non-slat windows and then demonstrated how slats can be used to attenuate the excessive daylight.

In our previous studies [4,5], an analytical model was developed to calculate the interior daylight illuminance from the slat window. The model could facilitate determining the reduced lighting power density of designated buildings for the annual energy consumption evaluation according to Thailand building energy code. The studies also showed that the daylighting from the slat window is cost effective in terms of the energy savings from installing the slat window coupled with the dimmable electric lighting system. However, the

studies did not examine the associated heat of the entering daylight that would become the air-conditioning load of the room.

In this paper, the energy performance of the daylighting from the slat window was studied. A thermal model of the slat window was developed and validated with experiments. The thermal model and the daylight model developed earlier were used to evaluate the lighting and air-conditioning energy consumptions of an office room equipped with the slat window. The consumptions were compared to that of the same room equipped with the heat reflective glass window to appraise the energy saving potential. By using the models, the slat angles that maximize the energy saving could be determined. The energy saving of a daylighting scheme that the beam radiation is completely shaded from entering the room was also evaluated in this study.

2. Heat transfer through the slat window

A non-steady heat transfer model was developed for the slat window. Fig. 1 shows the slat window model consisting of two adjacent slats located at the middle between two glass panes. The slats have a width of W_l and a separation of S_l and are tilted at an angle of φ_l measured with respect to the horizontal direction. The outer glass pane with a thickness of e_o is set apart at a distance of D from the inner glass panes with a thickness of e_i . The distance from the edges of the slats to the surfaces of both outer and inner glass panes is d .

In the figure, the heat transfer through the slat window (q_w) is analyzed based on mechanisms of radiation exchanges and heat convections. The analysis determines the net radiative energy absorbed (A') by the slats and the glasses from the exchanges of the solar (shortwave) and thermal (longwave) radiations within the air gap of the slat window. The analysis also determines the net energy absorbed due to the heat convection of the air within the gap between either side of the slat edge and the glass pane (A'').

The energy balances of the whole window system are simultaneously performed at the slats and the two glass panes by considering the incident solar radiations, the net absorbed energy from the heat exchanges within the air gap, and the heat convection on the glass surfaces by the surrounding air. In the energy balances, the effects of thermal storage are taken into account as a result of the slat and glass properties.

For the slat window, the slats can be rotated counterclockwise from the horizontal line at which the angle is measured as positive value ($+\varphi_l$). Rotating the slats clockwise from the horizontal line, the measured angle is assigned as negative value ($-\varphi_l$).

2.1. Solar (shortwave) radiative exchanges

As illustrated in Fig. 1, a fictive cavity is established for the analysis of the solar radiative exchanges within the air gap. The fictive

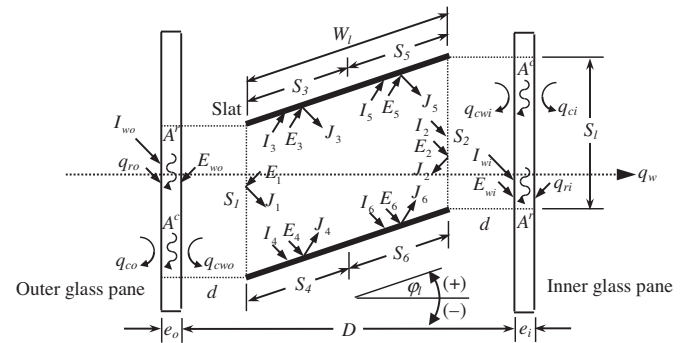
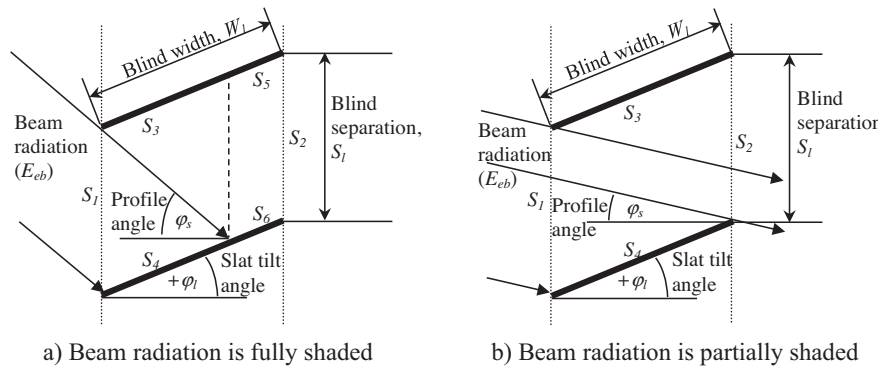


Fig. 1. The heat transfer model of the slat window.

**Fig. 2.** Incidences of beam radiation on the slat window.

cavity is enclosed by the slat surfaces of S_3 to S_6 and the fictive surfaces of S_1 and S_2 . In the analysis, the incident solar radiations on the surfaces are first determined. Fig. 2 shows the incidences of the beam normal radiation (E_{eb}) on the slat window at the slat angle of $+\varphi_l$.

The amount of the incident beam radiation on the slat surface S_4 (W/m^2) can be calculated as

$$I_4^b = \tau_{wo}(\eta_{wo}) \cdot E_{eb} \cdot \cos \eta_l, \quad (1)$$

where τ_{wo} is the solar transmittance of the outer glass pane. η_{wo} and η_l are the incidence angles of the beam radiation on the outer glass and on the slat, respectively. According to [4], the dependence of the glass transmittance on the incidence angle can be expressed as

$$\tau_{wo}(\eta_{wo}) = \tau_{wo}(0^\circ) \cdot [1.018 \cdot \cos \eta_{wo} \cdot (1 + \sin^3 \eta_{wo})], \quad (2)$$

where $\tau_{wo}(0^\circ)$ is the solar transmittance of the outer glass at the normal incidence. Eq. (2) can be applied for the incidence angle from 0° to 90° .

Examining Fig. 2(a), the beam radiation is completely shaded by the slats. The length of S_4 can be determined from the geometrical position of the sun relative to the slat:

$$S_4 = \frac{1}{\cos \varphi_l \tan \varphi_s + \sin \varphi_l} \cdot S_1, \quad (3)$$

where φ_s is the solar profile angle, defined as the angle between the outward normal of the window and the projection of the vector from the window to the sun on the vertical plane containing the outward normal, and can be written as

$$\varphi_s = \tan^{-1} \left(\frac{\tan \alpha_s}{\cos(\gamma_s - \gamma_W)} \right), \quad (4)$$

where α_s is the solar altitude angle and γ_s is the solar azimuth angle. γ_W is the azimuth angle of the window.

In the figure, the length of the sun shaded surface S_6 can be obtained by subtracting W_l by S_4 . The lengths of S_3 and S_5 are assigned equal to S_4 and S_6 , respectively. The lengths of S_1 and S_2 are both equal to S_l .

Fig. 2(b) shows another case where part of the beam radiation is intercepted by the slats and the other part directly reaches on the inner glass pane. In this case, the upper surfaces of the slats are fully sunlit, thus S_4 equals to W_l ($S_6 = 0$). The proportion of the sunlit area on the total area of the inner glass pane (F_b) can be determined by using the relationships presented in Table 1.

The average amount of the incident beam radiation on the inner glass surface S_2 (W/m^2) is thus calculated as

$$I_2^b = F_b \cdot \tau_{wo}(\eta_{wo}) \cdot E_{eb} \cdot \cos \eta_{wi}, \quad (5)$$

where η_{wi} is the beam incidence angle on the inner glass surface. The F_b value is obtained from the relationships in Table 3.

Table 1
Proportion of the sunlit area on the inner glass pane of the slat window (F_b).

Slat angle	Condition	Portion of the sunlit area on the inner glass pane
$\varphi_l \geq 0^\circ$	All values of φ_s	$F_b = 1 - \frac{W_l \sin \varphi_l}{S_l} - \frac{W_l \cos \varphi_l \tan \varphi_s}{S_l}$
$\varphi_l < 0^\circ$	$\varphi_s < \varphi_l $	$F_b = 1 - \frac{W_l \sin \varphi_l }{S_l} + \frac{W_l \cos \varphi_l \tan \varphi_s}{S_l}$
	$\varphi_s \geq \varphi_l $	$F_b = 1 + \frac{W_l \sin \varphi_l }{S_l} - \frac{W_l \cos \varphi_l \tan \varphi_s}{S_l}$

Table 2
Lower and upper limits of the elevation angle used to determine values of diffuse light from sky and ground incident on the six surfaces of the slats.

Blind segment	Visible part	Elevation angle (α)	
		Lower limit (α_{ll})	Upper limit (α_{ul})
S_1	Sky	n/a	n/a
	Ground	n/a	n/a
S_2	Sky	0	$\tan^{-1} \left(\frac{0.5 - B \sin \varphi_l}{B \cos \varphi_l} \right)$
	Ground	$-\tan^{-1} \left(\frac{0.5 + B \sin \varphi_l}{B \cos \varphi_l} \right)$	0
S_3	Sky	n/a	n/a
	Ground	$-\tan^{-1} \left(\frac{1 + 0.25B \sin \varphi_l}{0.25B \cos \varphi_l} \right)$	$-\varphi_l$
S_4	Sky	0	$\tan^{-1} \left(\frac{1 - 0.25B \sin \varphi_l}{0.25B \cos \varphi_l} \right)$
	Ground	$-\varphi_l$	0
S_5	Sky	n/a	n/a
	Ground	$-\tan^{-1} \left(\frac{1 + 0.75B \sin \varphi_l}{0.75B \cos \varphi_l} \right)$	$-\varphi_l$
S_6	Sky	0	$\tan^{-1} \left(\frac{1 - 0.75B \sin \varphi_l}{0.75B \cos \varphi_l} \right)$
	Ground	$-\varphi_l$	0

Table 3
Optical properties of the glass and the shading slats of the slat window.

Description	Green glass	Slat
Solar range	Transmittance	0.44
	Reflectance	0.05
	Absorptance	0.51
Visible range	Transmittance	0.74
	Reflectance	0.06
Infrared range	Emittance	0.84
		0.65

By assuming all the surfaces are perfectly diffusive, the solar radiative exchange due to the multiple reflections of the incident beam radiation can be resolved by

$$J_i^b = \rho_i I_i^b + \rho_i \sum_j J_j^b \cdot F_{ij}, \quad (6)$$

where J_i^b is the beam solar radiosities of surface i (W/m^2). ρ_i is the solar reflectance of surface i . F_{ij} is the view factor from surface i to surface j . I_i^b is the incident beam radiation on surface i (W/m^2).

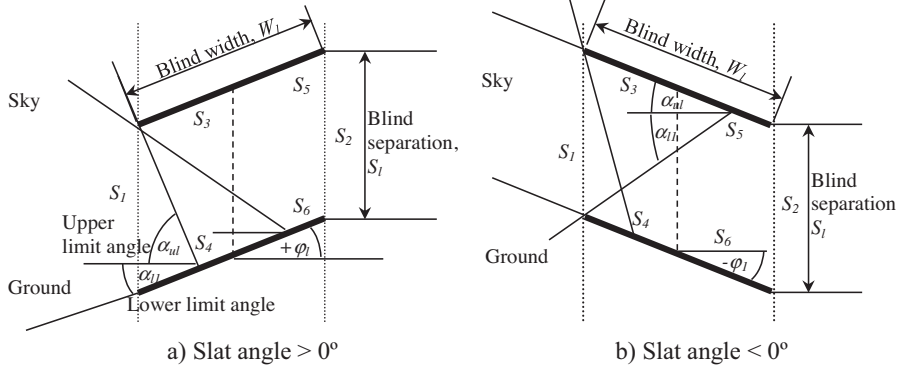


Fig. 3. Incidences of diffuse radiation on the slat window.

As a consequence, the beam solar irradiation on surface i (E_i^b) and the absorbed energy on surface i (A_i^b) can be obtained from

$$E_i^b = \sum_i J_i^b \cdot F_{ij}, \text{ and} \quad (7)$$

$$A_i^b = \alpha_i \cdot E_i^b, \quad (8)$$

where α_i is the solar absorptance of surface i .

By Eqs. (6)–(8), the calculated values of surfaces 1 and 2 are to be correspondent with the values of the outer glass and the inner glass, respectively (i.e. $J_{wo}^b = J_1^b$, $J_{wi}^b = J_2^b$, and $E_{wo}^b = E_1^b$, $E_{wi}^b = E_2^b$, and $A_{wo}^b = A_1^b$, $A_{wi}^b = A_2^b$). For the slats, its values can be obtained by averaging the calculated values of surfaces 3–6 weighted by the surface length

$$\left(\text{e.g. } J_l^b = \sum_{i=3}^6 J_i^b \cdot S_i / \sum_{i=3}^6 S_i\right).$$

The slats and the glasses also receive the diffuse radiations from the sky and the ground. Fig. 3 shows the incidences of the diffuse radiations. At this step, the lengths of S_3 , S_4 , S_5 and S_6 are all set equal to half of the slat width. The incident diffuse radiation on surface i (I_i^d) can be calculated as:

$$I_i^d = \int_{\gamma_w - \pi/2 \alpha_{ll}}^{\gamma_w + \pi/2 \alpha_{ul}} \int \tau_{wo}(\eta_{wo}) R \cos \eta_i d\alpha d\gamma \quad (9)$$

where R is radiance values of the sky or the ground. α_{ul} and α_{ll} are the lower and upper limits of the elevation angle of the surface for sky or ground-reflected radiation.

In Eq. (9), the radiance values (R) at any points over the sky can be calculated from the ASRC-CIE sky model that is suitable for our tropical sky [22]. Radiance value of the ground can be derived by dividing the reflected global radiation from ground by π .

According to the slat geometry at the positive tilted angle as shown in Fig. 4(a), values of the lower and upper limits of each surface in Eq. (9) can be exhibited as in Table 2. The variable B in the table represents the ratio of slat width to slat separation, $B = W_l/S_l$.

By substituting I_i^d for I_i^b in Eq. (6), and J_i^d for J_i^b in Eq. (7), and E_i^d for E_i^b in Eq. (8), the absorbed energy due to the incident diffuse radiation (A_i^d) can be obtained. Values of the form factors of the six surfaces are calculated in accordance with the configuration in Fig. 3. Finally, the total solar radiosity (J_w^s), total solar irradiation (E_w^s) and the solar energy absorbed (A_w^s) by the slats and the glasses due to the solar radiative exchange can be calculated as

$$J_w^s = J_w^b + J_w^d, \quad (10a)$$

$$E_w^s = E_w^b + E_w^d, \quad (10b)$$

$$A_w^s = A_w^b + A_w^d, \quad (10c)$$

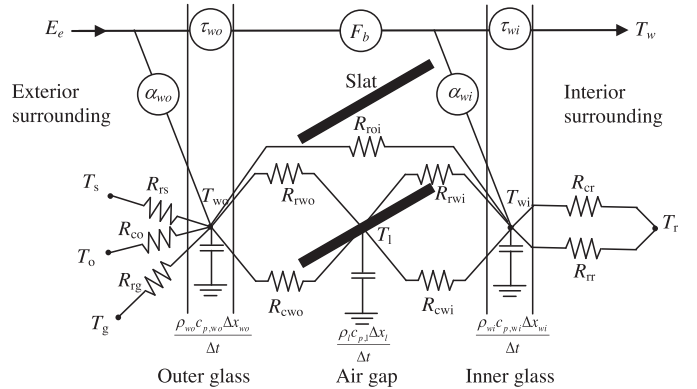


Fig. 4. The thermal resistance network of the slat window.

where w stands for the window components that are the outer glass (wo), the inner glass (mi) and the slat (l).

It should be noted that the limit values in Table 2 are to be applied in inverse way when the slats are tilted at the angle of negative values as shown in Fig. 3(b).

2.2. Thermal (longwave) radiative exchange

The fictive cavity is also applied for analyzing the thermal radiative exchange between the slats and the glasses. The six surfaces are assumed to be the gray-diffusive. By using the radiosity method, the thermal radiosities of the six surfaces can be written as

$$J_i^t = \varepsilon_i \sigma T_i^4 + (1 - \varepsilon_i) \sum_j J_j^t \cdot F_{ij}, \quad (11)$$

where J_i^t is the thermal radiosity of surface i (W/m^2). ε_i is the emittance of surface i . T_i is the temperature of surface i (K).

As the temperatures of the six surfaces are also unknown, an iterative process is used to obtain the solution of these non-linear equations. In the calculation, the temperatures of S_3 – S_6 are assigned with the same value and represent the slat temperature.

The net thermal energy absorbed by surface i (A_i^t) can be calculated from

$$A_i^t = E_i^t - J_i^t, \quad (12)$$

$$\text{where } E_i^t = \sum_j J_j^t \cdot F_{ij}.$$

At this moment, total radiative energy absorbed (A_w^r) by the slats and the glass panes can be obtained by summing absorbed solar and thermal radiations:

$$A_w^r = A_w^s + A_w^t, \quad (13)$$

where w stands for the outer glass (wo), the inner glass (wi) and the slat (l).

2.3. Convective heat exchange

Examining Fig. 1 again, the outer glass pane is also subjected to the heat convection by the outdoor air. The rate of the heat convection (q_{co}) can be calculated as

$q_{co} = h_{co}(T_o - T_{wo})$, (14) where T_o is the outdoor air temperature (K). T_{wo} is the surface temperature of the outer glass (K). h_{co} is the convective heat transfer coefficient ($\text{W}/(\text{m}^2 \text{K})$) determined by the relationships suggested by Finlayson et al. [23]

$$h_{co} = 8.07 \cdot V_o^{0.605}, \quad \text{for } V_o < 2 \text{ m/s, and} \quad (15a)$$

$$h_{co} = 12.27, \quad \text{for } V_o > 2 \text{ m/s,} \quad (15b)$$

where V_o is the velocity of the outdoor air (m/s).

For the inner glass pane, the glass itself is subjected to the heat convection by the room air (q_{ci}) that can be calculated as

$$q_{cr} = h_{cr}(T_{wi} - T_r), \quad (16)$$

where T_{wi} is the surface temperature of the inner glass (K). T_r is the room air temperature (K). h_{cr} is the forced convective heat transfer coefficient of the indoor air film ($\text{W}/(\text{m}^2 \text{K})$) for air-conditioned space defined as

$$h_{cr} = 5.6 + 3.8 \cdot V_r, \quad \text{for } V_r < 5 \text{ m/s} \quad (17)$$

where V_r is the air velocity in front of the window plane [24].

The natural air circulation within the air gap also causes the heat transfer between the slats and the glass panes. According to Collins et al. [25], the convective heat transfer (q_{cw}) can be calculated for either side of the slats and the glasses as follows:

$$q_{cw} = h_{cw}(T_w - T_l), \quad (18a)$$

$$h_{cw} = \frac{\text{Nu} \cdot k}{L}, \quad (18b)$$

$$\text{Nu} = \left[1 + \left(\frac{0.0665 Ra^{0.33}}{1 + (9000/Ra)^{1.4}} \right)^2 \right]^{0.5}, \quad (18c)$$

$$Ra = \frac{\rho^2 \cdot g \cdot \beta \cdot \Delta T \cdot L^3}{\mu^2} Pr, \quad (18d)$$

$$L = \frac{D - 0.70 \cdot W_l \cos \varphi_l}{2}, \quad (18e)$$

where T_w and T_l are the temperatures of the glass panes and the slats (K). h_{cw} is the convective heat transfer coefficient ($\text{W}/(\text{m}^2 \text{K})$). k is the thermal conductivity of the gas in the gap ($\text{W}/(\text{m K})$). Nu is the Nusselt number of the half-gap cavity. Ra is the half-gap Rayleigh number. Pr is the Prandtl number. W is the gap width (m). g is the gravitational acceleration (m/s^2). β is the coefficient of thermal expansion. ρ is the gas density (kg/m^3). μ is the gas viscosity ($\text{N s}/\text{m}^2$). ΔT is the temperature difference between the gas pane and the slats (K).

By substituting T_{wo} for T_w in Eq. (18a), the calculation determines the convective heat transfer between the outer glass and the slat (q_{cwo}). Similarly, substituting T_{wi} in the equation, the convective heat transfer between the inner glass and the slat (q_{cwi}) is calculated. In this study, the gas within the window gap is air, thus the values of the parameters relating to the gas in Eq. (18) can be assigned as follows: $k = 0.027$, $\rho = 1.13$, $\mu = 16.97 \times 10^{-6}$, and $Pr = 0.71$.

2.4. Energy balances of the slat window

Fig. 4 shows the thermal resistance network for the energy balance analysis of the slat window system. The analysis is to be simultaneously performed at the outer glass pane, the slats, and the inner glass panes to determine their temperature values. Due to the high thermal conductance of the glasses and the slats, the temperatures of each component can be represented with a single value. As shown in the resistance network, the thermal storage effect of each window component is included in the analysis.

2.4.1. The outer glass (Node T_{wo})

In Fig. 4, the front surface of the outer glass pane is subjected to the incident solar radiation (I_{wo}), the radiative exchanges with the sky (q_{rs}) and the ground (q_{rg}) and the heat convection by the outdoor air (q_{co}). The back surface of the glass is subjected to the radiative exchanges and natural heat convection within the air gap. Equation 19 expresses the formulation of the energy balance at the outer glass:

$$\begin{aligned} \alpha_{wo} I_{wo} + \frac{T_o - T_{wo,t}}{R_{co}} + \frac{T_s - T_{wo,t}}{R_{rs}} + \frac{T_g - T_{wo,t}}{R_{rg}} + A_{wo}^r \\ = \frac{T_{wo,t} - T_{l,t}}{R_{cwo}} + \frac{\rho_{wo} C_{p,wo} x_{wo}}{\Delta t} (T_{wo,t} - T_{wo,t-1}) \end{aligned} \quad (19)$$

where I_{wo} is the incident solar radiation on the outer glass. T_o is the outdoor air temperature (K). T_s is the sky temperature (K). T_g is the ground surface temperature (K). $T_{wo,t}$ and $T_{wo,t-1}$ is the outer glass temperature at time t and $t - 1$ (K), respectively. $T_{l,t}$ is the slat temperature at time t . ρ_{wo} is the density of the outer glass (kg/m^3). $C_{p,wo}$ is the specific heat capacity of the outer glass ($\text{kJ}/(\text{kg K})$). x_{wo} is the glass thickness (m). Δt is the calculation time step (s). R_{co} is the thermal resistance of the convective heat transfer between the outer glass and the outdoor air, and can be expressed mathematically as the reciprocal of h_{co} ($R_{co} = 1/h_{co}$). R_{cwo} is the thermal resistance of the heat transfer between the outer glass and the slat by the natural air convection ($R_{cwo} = 1/h_{cwo}$). R_{rs} and R_{rg} are thermal resistance of the radiative heat transfer between the outer glass and the sky and between the outer glass and the ground, respectively. A_{wo}^r is the net energy absorbed by the outer glass due to the radiation exchange within the air gap.

2.4.2. The slats (Node T_l)

In this model, the slats are subjected to the solar and thermal radiative heat exchanges and the convective heat exchanges with the two glass panes. The energy balance at the slats can be formulated as

$$A_l^r + \frac{T_{wo,t} - T_{l,t}}{R_{cwo}} + \frac{T_{l,t} - T_{wi,t}}{R_{cwi}} = \left(\frac{\rho_l C_{p,l} x_l}{\Delta t} \right) (T_{l,t} - T_{l,t-1}), \quad (20)$$

where ρ_l is the density of the slat (kg/m^3). $C_{p,l}$ is the specific heat capacity of the slat ($\text{kJ}/(\text{kg K})$). x_l is the thickness of the slat (m). $T_{l,t}$ and $T_{l,t-1}$ is the slat temperature at time t and $t - 1$ (K), respectively. A_l^r is the net energy absorbed by the slats due to the radiation exchange within the air gap. R_{cwi} is the thermal resistance of the heat transfer between the slat and the inner glass by the natural air convection ($R_{cwi} = 1/h_{cwi}$).

2.4.3. The inner glass (Node T_{wi})

For the inner glass, its front surface is subjected to the radiative exchange and the convective heat transfer within the air gap and also receive the direct-transmitted solar radiation. The back surface of the glass is subject to the interior thermal environment of the room through the convection and radiation. The energy balances

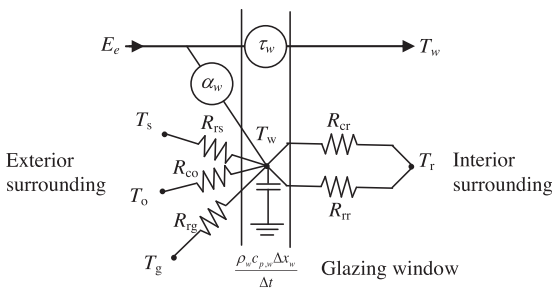


Fig. 5. The thermal resistance network of a single-pane glazed window.

can be formulated as

$$\begin{aligned} \alpha_{wi} I_{wi} + \frac{T_{l,t} - T_{wi,t}}{R_{cwi}} + A_{wi}^r &= \frac{T_{wi,t} - T_r}{R_{cr}} \\ + \frac{T_{wi,t} - T_r}{R_{rr}} + \left(\frac{\rho_{wi} c_{p,wi} x_{wi}}{\Delta t} \right) (T_{wi,t} - T_{wi,t-1}), \end{aligned} \quad (21)$$

where I_{wi} is the incident solar radiation on the inner glass. ρ_{wi} is the density of the inner glass (kg/m^3). $c_{p,wi}$ is the specific heat capacity of the inner glass ($\text{kJ}/\text{kg.K}$). x_{wi} is the thickness of the inner glass (m). $T_{wi,t}$ and $T_{wi,t-1}$ are the inner glass temperatures at time t and $t-1$ (K), respectively. A_{wi}^r is the net energy absorbed by the inner glass due to the radiation exchange within the air gap.

Now, the temperatures of the slats and the glasses and the resulting heat transfer can be calculated by solving the energy balance equations of the whole window system. At a particular time t , the solar radiation exchanges within the air gap are first analyzed by using Eqs. (1)–(10), and the values of A_{wi}^s are obtained as the result. The unknown values of the slat and the glass temperatures are then assumed for the analysis of the thermal radiative and convective exchanges within the air gap. The analysis is performed by using Eqs. (11)–(18) and the values of A_{wi}^t and q_{cw} are obtained as the result. All calculated values are next substituted into Eqs. (19)–(21) to evaluate their satisfactions.

At this step, an iterative process of Newton-Raphson method is applied to produce the new estimated values of the slat and the glasses for their new assumed values in the next iteration round. New temperatures of the slat and the glasses are calculated by using the heat flux residuals (Δ_i) and their derivatives with respect to temperatures ($\partial \Delta_i / \partial T_j$). The heat flux residuals (Δ_i) are obtained by subtracting the calculated values of the left hand side terms with the right hand side terms of Eqs. (19)–(21). The temperature derivatives of the heat flux residuals are complicated due to nonlinear dependence of the heat transfer residual equation on the temperatures. These expressions are calculated numerically by using central difference approximation method. The process will be repeated until the energy balance equations are satisfied. For this model, the convergence criterion is set at the residual sum from energy balances on both glasses and the slats less than 0.05 W. After obtaining the temperature values, the total heat transfer through the slat window (q_w) can be calculated as

$$q_w = \tau_{wi} \cdot E_{wi}^s + q_{cr} + q_{rr}, \quad (22)$$

where E_{wi}^s is the total solar irradiation on the front surface of the inner glass pane. q_{cr} and q_{rr} are the convective and radiative heat transfer between the back surface of the inner glass pane and the room interior.

2.5. A model for a single-pane glazed window

In this study, a model of a single-pane glazed window was also developed to facilitate the determination of the thermal performance of the heat reflective glass. Fig. 5 shows the thermal

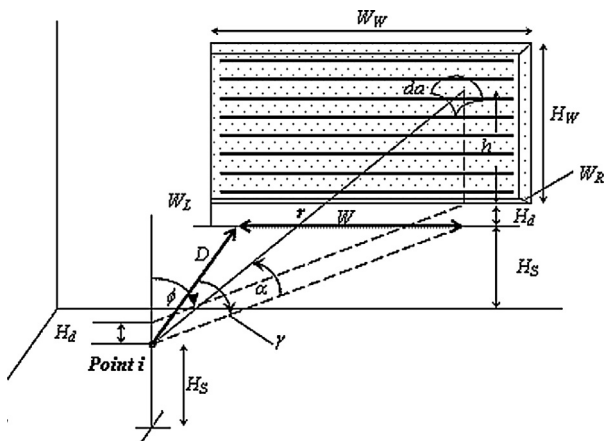


Fig. 6. Light flux from a patch of window reaching segment i on interior room surface.

resistance network of the model. Compared with Fig. 4, the model excludes the heat exchanges within the air gap, but the other parts are all identical.

3. Daylight from the slat window

In this study, the daylight model developed in our previous works was adopted to determine the interior workplane daylight from the slat window [4,5]. The model requires the coordinates of the window and of the room as the input. The interior surfaces (wall, floor and ceiling) of the room are first divided into a number of small segments to determine the daylight distribution by using Eq. (23):

$$E_{di} = \int_{\gamma} \int_{\phi} L_w \cos \eta \sin \phi d\phi d\gamma. \quad (23)$$

In Eq. (23), E_{di} is the daylight from the slat window that directly reaches on the surface segment i . L_w represents the window luminance that varies with the line of sight from point i to the patch da on the window as shown in Fig. 6.

Value of L_w is obtained as the weighted average between the luminance of the exterior source (sky or ground) and that of slat surface (either lower or upper surface). The luminance value of a patch of sky can be computed using ASRC-CIE sky model [22]. The luminance values of the upper and lower slat surfaces are calculated from reflections of lights from the sun, the sky and ground on the slat surfaces and the two panes of the glazed window. η stands for the angle of incidence between the line of sight and the normal to plan of the wall segment. ϕ and γ are angular variables defined by the window configuration.

For the distribution of the non-slat-reflected sunlight from the slat window onto the interior room surfaces, the daylight model simply determined using Eq. (24)

$$E_{si} = \tau_{wo} \cdot \tau_{wi} \cdot F_b \cdot E_{vb} \cdot A_w \cdot \frac{\cos \eta_i}{\sum_{j=1}^n A_j \cdot \cos \eta_j}. \quad (24)$$

In the equation, E_{vb} stands for the sunlight on the outer glass pane. τ_{wo} and τ_{wi} are the visible transmittances of the outer and inner glazed windows, respectively. A_w is the window area. A_j is the area of the sunlit segment j . η_i is the incident angle of the sunlight on the segment i , and n is the total number of the segments in the room lit by the sunlight. In the equation, F_b represents a fraction of the sunlit area to the total window area that the value can be obtained from Table 2. A surface segment is assumed to receive the sunlight

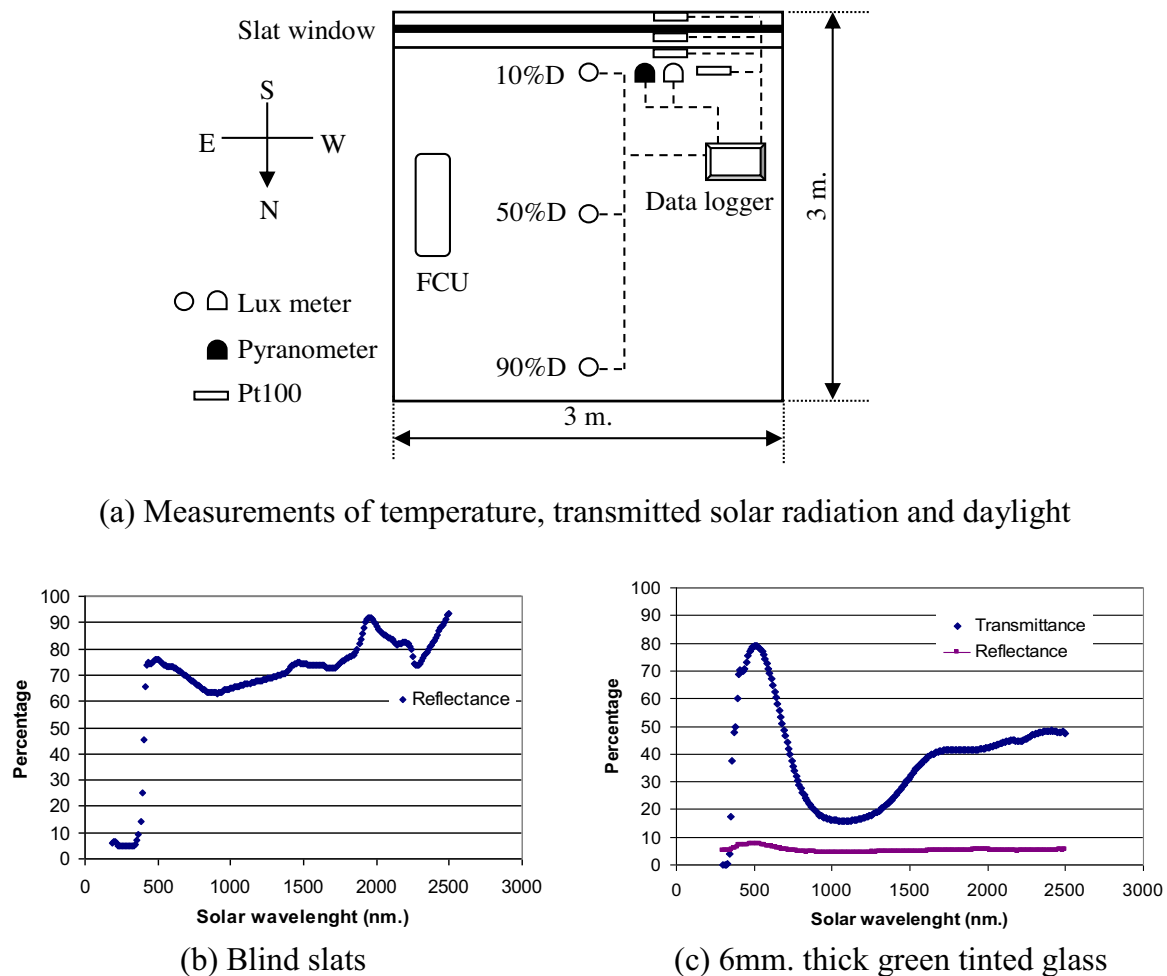


Fig. 7. The experimental setup.

if a line drawn from the center point of the segment to the sun is within the field of view from the point to the window scene. The total direct illuminance from the window on segment i (E_i) can be calculated as the sum of E_{di} and E_{si} .

To deal with the exchange of the light flux by multiple reflections between the small segments of the room interior surfaces, form factors are calculated for the whole segments. The form factors are then used in radiosity method in determining the internally reflected components of the daylight and the total daylight illuminance on the segments. In the final step, the configuration factors between points on the work plane and the segments are determined and used to calculate the workplane daylight illuminance.

4. Experimental method

A series of full-scale experiments were conducted to investigate the thermal characteristic of a slat window. The experimental results were also used to validate the thermal model of the slat window in Section 2, implemented by coding in Visual Basic 6 program. Fig. 7(a) shows the experimental setup. The experimental facilities, equipment and measurements are described below.

4.1. The experimental room

The experimental room was a 3.0 m by 3.0 m room with a 2.65 m height. The room was located at Bang Khun Tien campus of King Mongkut's University of Technology, Thonburi (latitude 13.57°N and longitude 100.44°E). The room had a 6 mm green glass win-

dow on the south wall. The window was 2.8 m wide by 1.5 m high and its sill was 0.85 m above the floor. The interior wall surfaces were painted white with a reflectance value of 0.73. The surface reflectance of the ceiling and floor was measured at 0.73 and 0.43, respectively. A fan coil unit was installed for the room air-conditioning.

4.2. The slat window

The slat window used in the experiments was formed by mounting a set of venetian blinds behind the existing green glass and then affixing with another set of the same glass. The measured distance between the two glass panes was 10 cm. The blind slats were 5.0 cm wide and white-painted aluminum. The distance between two adjacent slats was 4.2 cm. The optical properties of the glass and the slats are summarized in Table 3. Their spectral transmittance and reflectance were shown in Fig. 7(b) and (c), respectively.

4.3. Measurement sensors

In the experiments, Platinum RTD (Pt100) sensors were used to measure the surface temperatures of the glass panes and a slat, and the temperature of the room air. All the Pt100 sensors were shaded from the direct incidence of beam radiation to reduce the measurement error of the surface temperatures. A pyranometer (KIPP & ZONEN: model CMP 11) was placed vertically behind the inner glass pane to measure the transmitted solar radiation. An illuminance sensor (EKO: model ML-020S-O) was also placed vertically

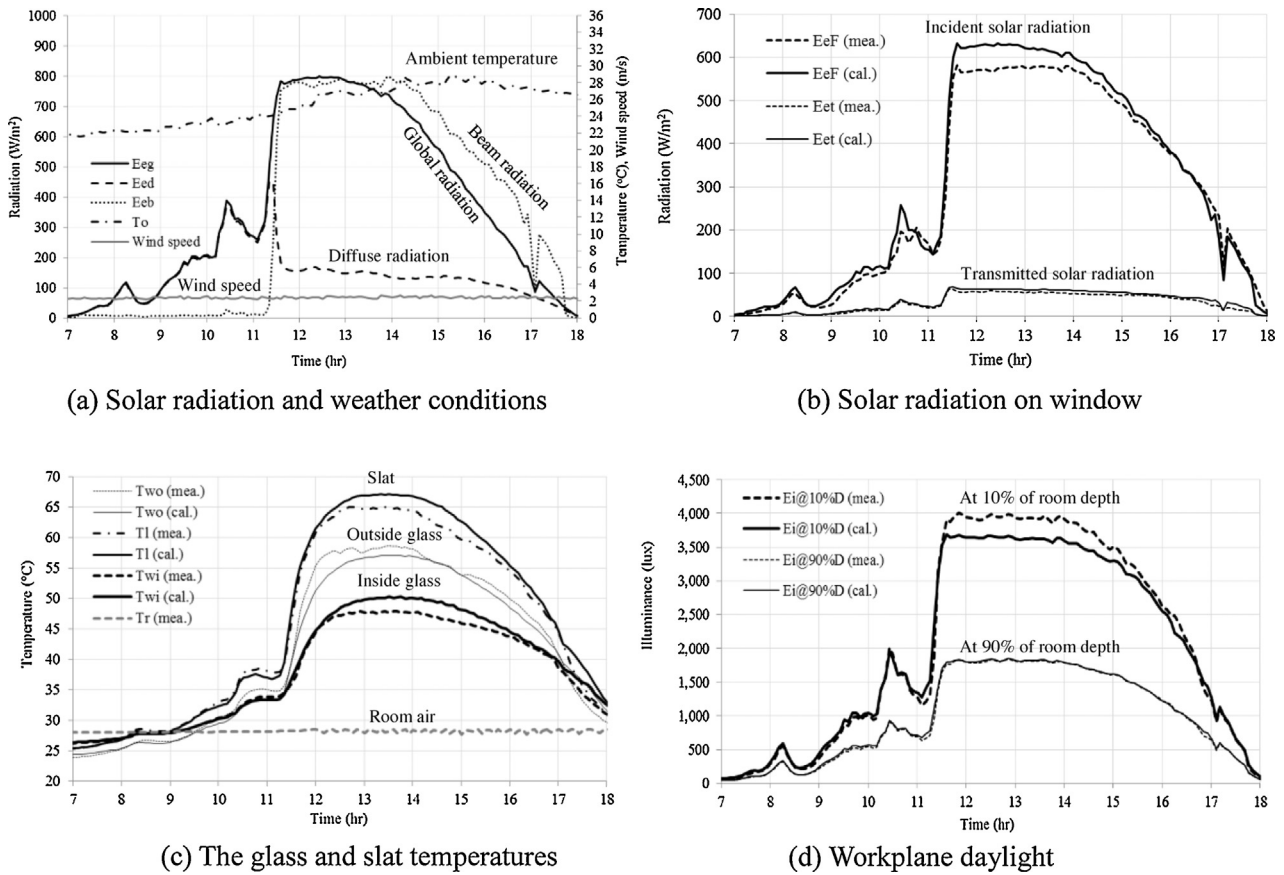


Fig. 8. Experiment of the slat window at the 0° angle (13/01/2014).

beside the pyranometer to measure the corresponding daylight transmission. The daylight illuminances on the work plane level (0.75 m above the floor) were measured at three points located on a line perpendicular to the windowed wall across the center of the room. The points were positioned along the line at 10%, 50%, and 90% depths of the room (D). A data logging system was used to acquire all measured data from the sensors every five minutes. For the indoor air velocity, a spot measurement was made near the inner glass surface using a portable hot wire anemometer.

4.4. The meteorological station

During the experiments, the exterior solar radiations, daylight illuminances and wind speed were measured and recorded at a meteorological station located on the roof deck of a seven-story building of the school of bioresources and technology in the university campus. The measured radiations and daylights included the global, diffuse horizontal and beam normal components. The measurements were also simultaneously made for the four cardinal orientations (North, East, South and West). The clock times of the data loggers at the station and at the experimental room were synchronized.

5. Experimental results

A set of experiments was conducted to validate the thermal model in Section 2. The measured surface temperatures of a slat and the glass panes were compared to that from the calculations. The transmitted solar radiation through the slat window was measured and compared, as well. In the calculations, the radiation records at the meteorological station and the measured temperatures of

the outdoor air and the room air were used as the input. In the experiments, the interior daylight illuminances were measured and compared to the calculated results from the daylight model developed in our prior works [4,5].

5.1. The slats at 0°

The first experiment was carried out for the 0° slat angle (fully open). Fig. 8(a) shows the five-minute records of the global (E_{eg}), diffuse horizontal (E_{ed}) and beam normal (E_{eb}) solar radiations on the experimental day (13 January, 2014). On this day, the sky was cloudy in most period of the morning. The sky became clearer after 11:15, and the beam radiation raised rapidly to 800 W/m^2 , while the diffuse component decreased below 200 W/m^2 . The outdoor air temperature (T_0) varied from 22°C to 29°C . The wind velocity varied between 2.1 m/s and 2.7 m/s .

Fig. 8(b) shows the measured solar radiation on the outer glass of the slat window ($E_{eF(meas.)}$). The value was obtained from the solar radiation on the south measured at the station added with the ground-reflected radiation. The addition term was estimated by multiplying the measured global radiation with the ground reflectance and the view factor between the ground and the windowed wall. The plot shows that the radiation on the window raised sharply to 580 W/m^2 by the incident beam radiation. However, with the sun shading by the slats, the transmitted radiation ($E_{eT(meas.)}$) was measured at 64 W/m^2 ; equivalent to 11% of the total radiation incidence. Although the solar elevation was rather low in this month, the calculation indicated that the slats at this position (0°) could fully shade the beam radiation during 9:30–16:00, covering 80% of the office hours (8:00–17:00).

Table 4

Evaluation of the calculation performance of the proposed slat window model.

Slat angle	StatisticalEvaluator	E_{eF} (W/m ²)	E_{eT} (W/m ²)	T_{wo} (°C)	T_l (°C)	T_{wi} (°C)	$E_{i@10\%D}$ (lx)	$E_{i@90\%D}$ (lx)
0°	MBD	16.59	4.19	-0.72	0.95	0.85	-88.22	13.30
	RMSD	31.81	13.58	1.56	1.60	1.31	180.74	23.73
30°	MBD	26.51	3.97	-0.55	1.38	0.72	-58.49	-53.63
	RMSD	41.77	4.29	1.61	1.68	0.94	99.31	76.97
-30°	MBD	24.04	-4.01	0.02	1.07	0.61	243.00	95.39
	RMSD	47.61	7.66	1.10	1.29	0.79	396.15	139.56

Note: MBD = $\frac{1}{N} \sum_{i=1}^N (C_i - M_i)$ and RMSD = $\sqrt{\frac{1}{N} \sum_{i=1}^N (C_i - M_i)^2}$ where C_i is the value computed from the model, M_i is the corresponding values from measurement, and N is the number of data.

Fig. 8(b) also shows the calculated radiations incident on ($E_{eF(cal.)}$) and transmitted through ($E_{eT(cal.)}$) the slat window. A correspondence between the calculations and the measurements can be observed. As exhibited in **Table 4**, the model slightly overestimates the incident radiation with the mean bias difference value (MBD) of 16.59 W/m². The root mean square difference value (RMSD) is 31.81 W/m². For the transmitted radiation, the MBD and RMSD values are 4.19 W/m² and 13.58 W/m², respectively.

Fig. 8(c) shows the measured temperatures of the slat ($T_{l(meas.)}$) and the outer and inner glass panes ($T_{wo(meas.)}$ and $T_{wi(meas.)}$). Examining their profiles, the temperatures varied with the incident radiation and were moderated by the thermal storage effect. In shading the sun, the slats received a large amount of solar radiation. As the transfer of the absorbed heat from the slats located within the non-ventilated air cavity was low, the slat temperature raised upto 65 °C during the experiment. This peak value was considerably high compared with the results of some similar studies in moderate climate [26–28]. In the figure, the temperature values from the calculations ($T_{l(cal.)}$, $T_{wo(cal.)}$ and $T_{wi(cal.)}$) were also plotted for the comparison. On average, the temperature differences between the calculations and the measurements are within ±1.0 °C. The measured room air temperature ($T_{r(meas.)}$) was also given in the figure.

In the experiment, the heat transfer from the window was not measured but the estimation could be made by calculations using the measured temperatures of the inner glass pane and the room air. At the time during the high solar incidence, the temperature of the inner glass reached 48.0 °C. The room air was measured at 28.3 °C. The convective heat transfer was calculated at 113.9 W/m². According to Eq. (17) and the measured air velocity of 0.05 m/s, the convective heat transfer coefficient (h_{cr}) of 5.8 W/m²/K was used in the calculation. For the radiative heat transfer, the calculations were made by simply assuming the temperature of the room interior surfaces equal to the room air temperature. The emittance of the interior surfaces was assumed at 0.80 W/m²/K. By the assumptions, the radiative heat transfer was estimated at 131.7 W/m². The above calculations indicate that by the shading, the transmitted solar radiation shared a minority in the total thermal gain.

Fig. 8(d) shows the workplane daylight illuminance at 10% and 90% of the experimental room depth ($E_{i@10\%D(meas.)}$ and $E_{i@90\%D(meas.)}$). Because the room was as shallow as 3 m, the depths at 10% and 90% were correspondent with 0.2 and 1.8 times of the window height (1.5 m). At both measurement points, the daylight illuminances were higher than a recommended workplane illuminance of 500 lx for most time during the office hours. However, the daylight value near the windowed wall was considered to be excessive when evaluated by using the “useful daylight illuminance” index that the workplane daylight should be not exceeding 2000 lx [29]. With the slat shading, the workplane daylight did not vary as substantially as the incident radiation. The figure also shows the workplane

daylights from the calculations ($E_{i@10\%D(cal.)}$ and $E_{i@90\%D(cal.)}$); the results compared well with the measurements.

5.2. The slats at 30°

Another experiment was carried out for the slats at 30°. **Fig. 9(a)** shows the solar radiations on the experimental day (15 January, 2014). As shown, the sky was clear throughout the day. The solar radiations in the afternoon were comparable with that of the previous experiment.

Fig. 9(b) shows that the incident solar radiation on the window was as high as 550 W/m² during noon. However, as it was intercepted by the slats with large amount, the transmitted radiation was at 31 W/m², about half of the measured peak in the first experiment. No beam radiation passed directly through the slat openings during this experiment.

The temperatures of the slat and the glasses were shown in **Fig. 9(c)**. For the inner glass, the temperature was peak at 46.1 °C, and the convective and radiative heat gains were estimated at 103.1 W/m² and 120.0 W/m², respectively. The values were marginally lower than those corresponding values calculated in the previous experiment.

Fig. 9(d) shows the workplane daylight illuminances. The illuminance values reduced proportionally with the reduced transmitted solar radiation. As the experimental room was shallow, tilting the slats to 30° still maintained the daylight illuminance above 500 lx at both measurement points, whilst reducing the window heat gain. The uniformity of the daylight distribution was also improved. In comparing the results of this experiment with the first experiment, although the amount of the total heat transfer decreased, the amount of the heat gain per unit of the daylight flux increased.

5.3. The slats at -30°

The last experiment is presented for the -30° angle. The measured global and diffuse radiations are shown in **Fig. 10(a)**. Although the experiment was undertaken on a different day (21 February, 2014), the solar radiations looked comparable to those of the first experiment where the sky was cloudy in the morning and rather clear in the afternoon. On this day, the global radiation reached 950 W/m² during 12:45–13:45. The outdoor temperature varied between 26 °C and 34 °C which was 2–5 °C higher than that of the previous two experiments.

Fig. 10(b) shows the measured incident and the transmitted solar radiations of the slat window. In the figure, while the incident radiation was at 526 W/m², the corresponding value of the transmitted radiation was at 88 W/m². At this slat position (-30°), more solar radiations from sky and from the reflection of the beam component on the slats surface could enter through the slat window into the room.

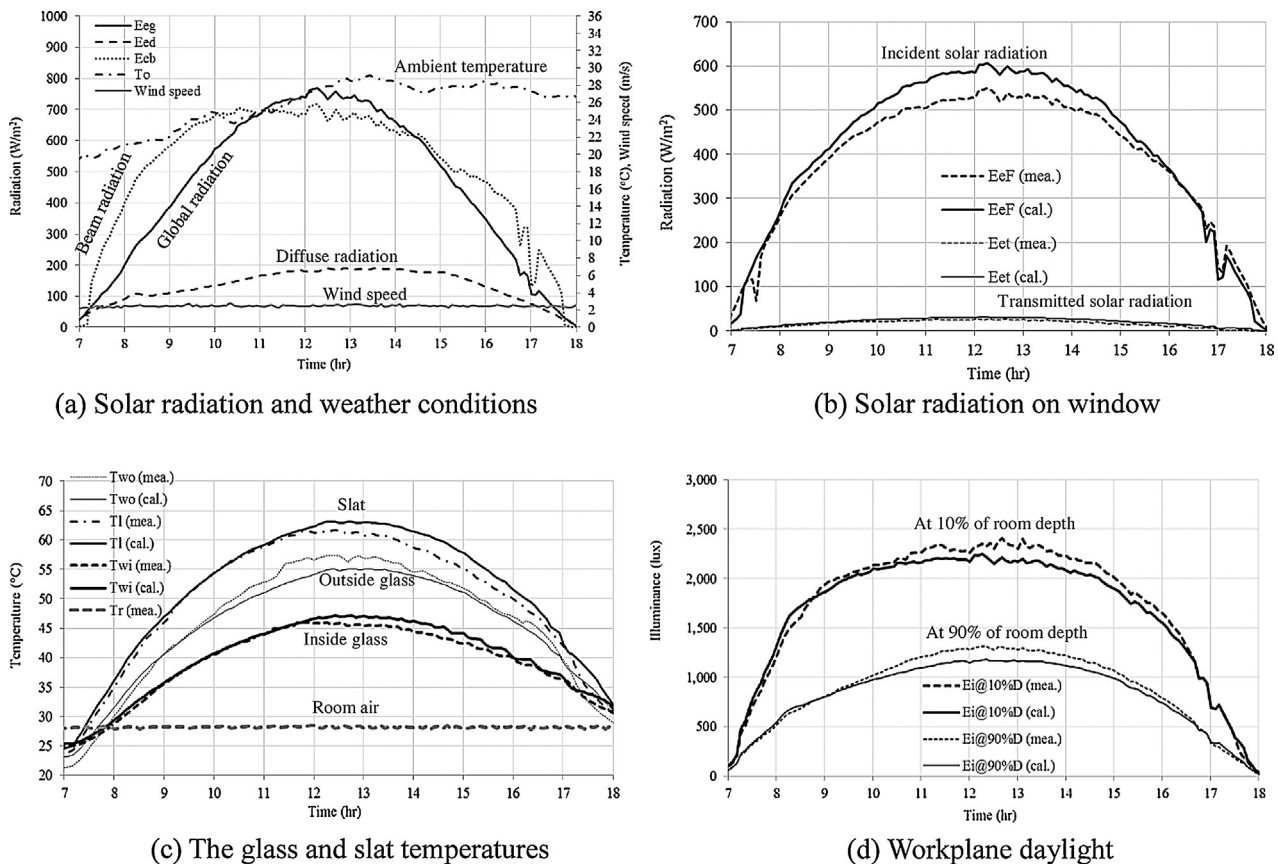


Fig. 9. Experiment of the slat window at the 30° angle (15/01/2014).

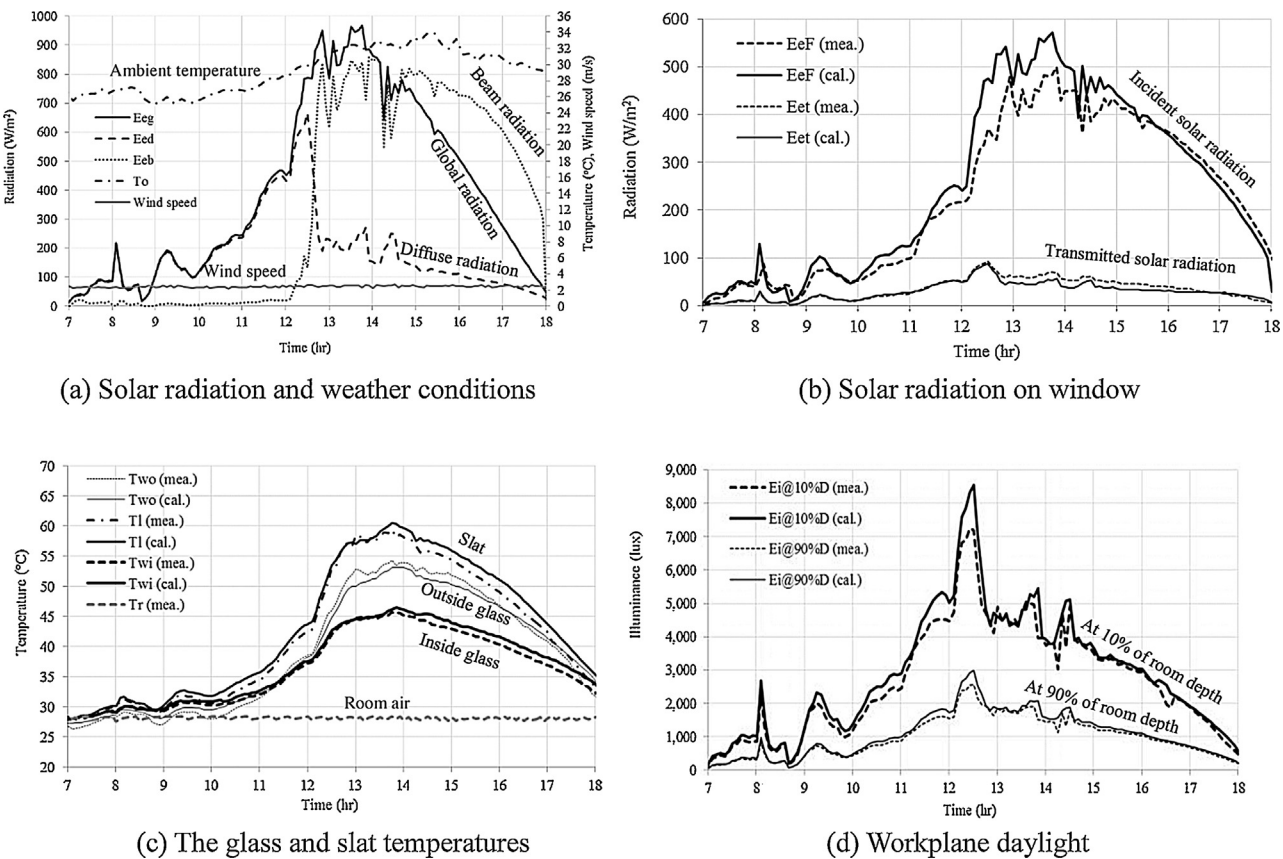


Fig. 10. Experiment of the slat window at the -30° angle (21/02/2014).

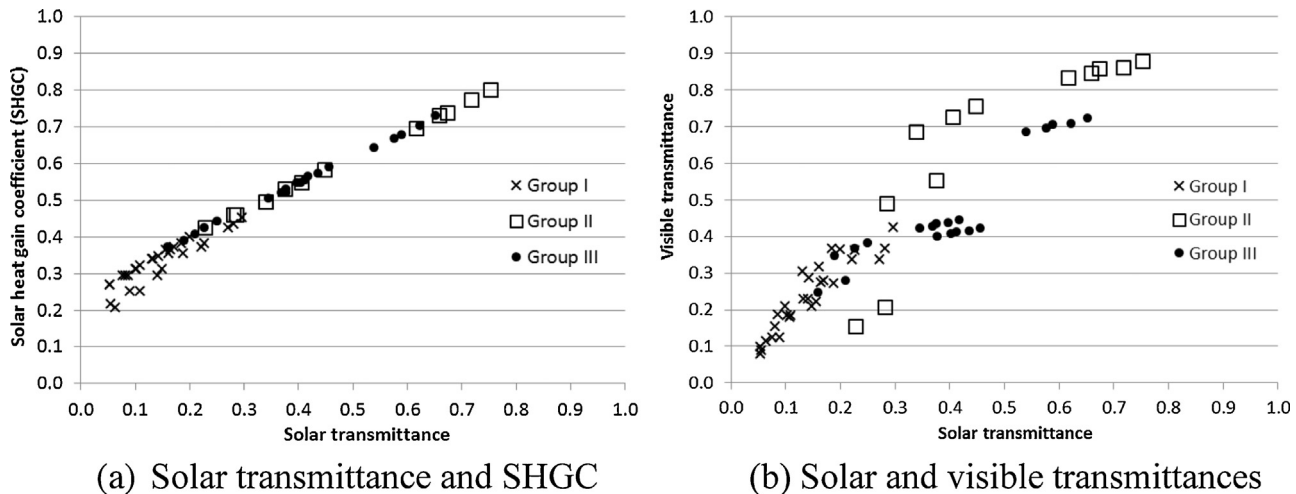


Fig. 11. Properties of the laminated glasses supplied by a manufacturer in Thailand.

Fig. 10(c) shows the variations of the slat and the glass temperatures. It is observed that the peak temperature of the inner glass did not much differ from the previous measurements. At this angle, the transmitted radiation would share with a larger portion in the total thermal gain compared to those of the first two experiments.

In **Fig. 10(d)**, the measured workplane daylights are shown. Although the slats turned toward to the sky, the sunlight was completely shaded during 9:00–16:00. More daylight from the sky could be transmitted through the openings. Distinct from the first experiment, the workplane daylights varied in a similar pattern with the exterior diffuse component, instead of the total incident radiation. The total heat gain per unit of the transmitted daylight flux would be smallest compared to those of the previous two experiments.

The three experiments exhibit a good application of the slat window for daylighting in our tropical region. As the solar elevation is high for most of the day time, the beam radiation can be largely intercepted during the office hours with shallow slat angle. The slats can also be tilted toward the sky to bring more diffuse daylight and redirect the incident sunlight into the room interior. For buildings in the tropics that are air-conditioned only by cooling, glasses with high visible transmittance and low solar absorptance improve the slat window performance by enhancing the daylight transmission and reducing the heat accumulation from the incident radiation. The slat with high solar reflectance and low solar absorptance also benefits the slat window. According to the evaluation results in **Table 4**, the thermal model predicted well the solar transmission and temperatures of the slat window under the exposure of varying solar radiation and surrounding condition.

6. Simulation-based analysis

After the experimental validation, the thermal model and the daylight model were used to evaluate the energy performance of the daylighting of a room equipped with the slat window. The modeled room was similar to the experimental room but its depth was extended to 15 m (10 times of the window height (H_w))). Reflectance values of the room interior surfaces were set at 0.7 for ceiling, 0.5 for walls and 0.3 for floor identical to those in the IES Lumen method for daylight calculation [30]. The exterior ground reflectance was assumed at 0.05. There was no change for the slat properties.

According to the Thai's regulation for building safety, the fabricated glasses for windows of buildings taller than 23 m must be laminated type. **Fig. 11** shows the properties of the laminated glasses supplied by a large manufacturer. Each point in the figure

represents a model of the laminated glasses that can be categorized into one of the three groups. The glasses in Group I are the heat reflective type with low solar transmittance and low solar heat gain coefficient (SHGC) (see **Fig. 11(a)**). These glasses are widely used for windows to prevent the excessive solar gain. Observing **Fig. 11(b)**, the glasses also have low visible transmittance.

Group II is the laminated clear glasses and the laminated tinted glasses. Compared to Group I, most of the glasses in Group II have higher solar transmittance and solar heat gain coefficient. The visible transmittance is also high that allows the daylight admission. For Group III, the glasses are actually those in Group II affixed with films. In this analysis, a model of the glasses in Group I was chosen to represent the typical glass windows of high-rise commercial buildings. Laminated glasses in Group II were chosen for the slat window. **Table 5** summarizes the values of the optical properties of the glasses selected for the simulations. The values were acquired from a product catalog given by a glass manufacturer.

The simulations were performed for the room with the slat window facing south and for the room with the slat window facing north. In the simulations, the slats were rotated from the angle of -50° to 50° , stepped up every 10° . The room air temperature was assumed constant at 25°C . The five-minute records of the solar radiation, daylight illuminance and ambient air condition at our meteorological station were used in the simulations.

6.1. The south facing slat window

The simulation results of the south facing slat window are first presented that comprise the solar and thermal gains, the daylight transmission, and the resulting energy consumptions of the lighting and air-conditioning of the modeled room. The results are also evaluated in comparison with the heat reflective glass.

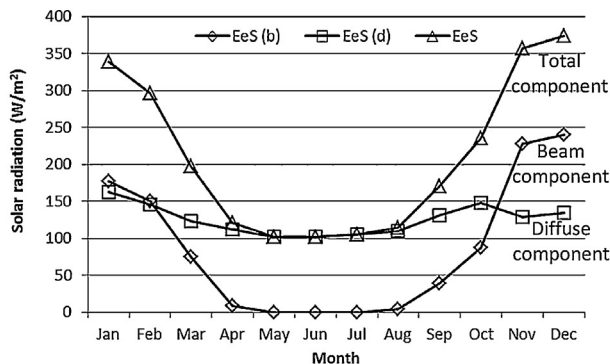
6.1.1. Solar and thermal gains

Fig. 12(a) shows the monthly average value of the incident solar radiation (E_{es}) on the outer glass of the slat window. The value was calculated based on the working hours during 8:00–17:00. It is observed that the value of the diffuse component of the incident radiation ($E_{es(d)}$) varies from 100 W/m^2 up to 160 W/m^2 over the year. For the beam component ($E_{es(b)}$), the incidence value depends on the sun position relative to the window orientation. The beam incidence is none from May till August, as the sun is due north. However, its value arises in the remaining months and is highest at 245 W/m^2 in December when the sun appears in front of the window at low elevation. In the figure, the total incident radiation

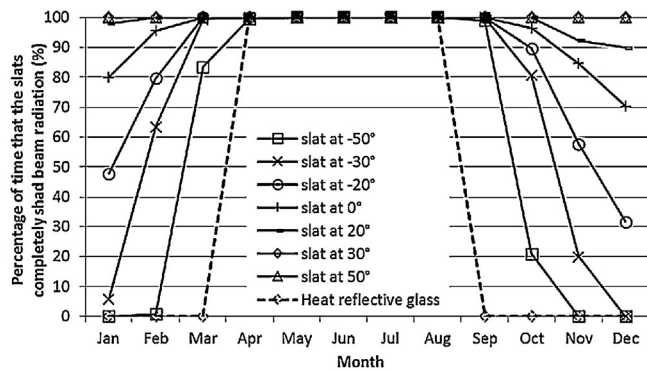
Table 5

Optical properties of the laminated glasses selected for the simulation study.

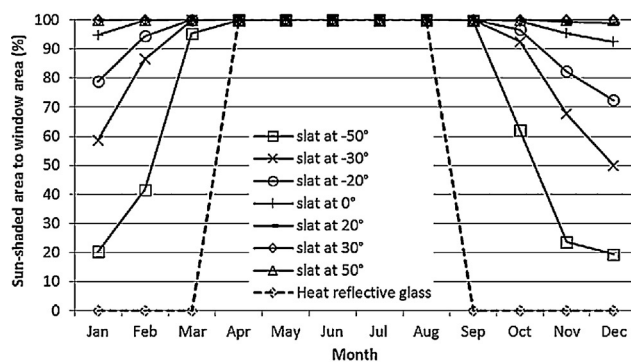
Description		Typical window	The slat window	
Glass type		Heat reflective (Single pane window)	Green-Clear (Outer glass pane)	Clear-Clear (Inner glass pane)
Solar range	Transmittance	0.06	0.41	0.75
	Reflectance	0.33	0.05	0.07
	Absorptance	0.61	0.54	0.18
	Transmittance	0.09	0.73	0.87
	Reflectance	0.32	0.07	0.07
	Emittance	0.85	0.85	0.85



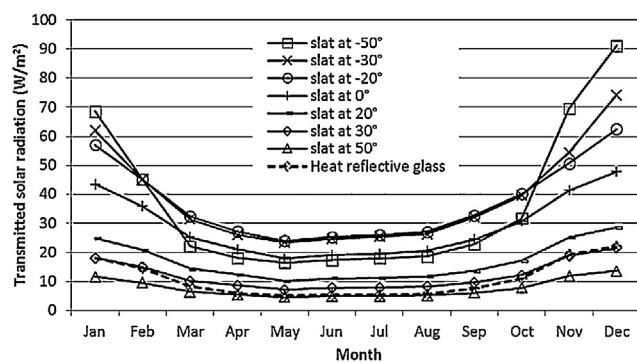
(a) Incident solar radiation on window



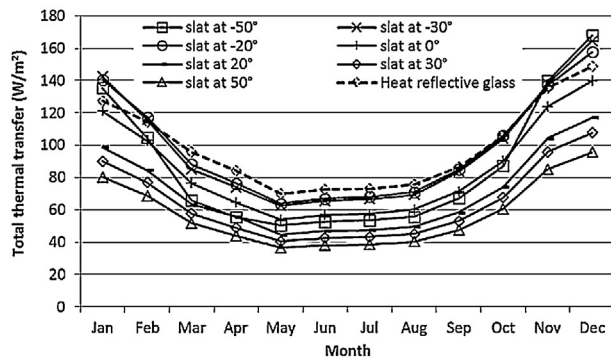
(b) The fully sun-shaded period



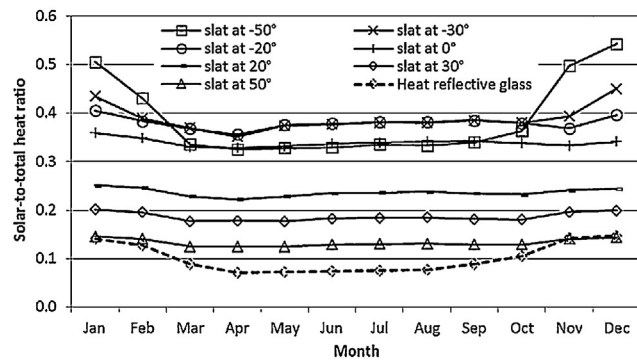
(c) Sun-shaded area to window area



(d) Transmitted solar radiation



(e) Total thermal gain



(f) Solar-to-total heat ratio

Fig. 12. Thermal simulations of the slat window facing south.

varies from 100 W/m² up to 370 W/m². In our study site where the sun always travels overhead and clouds present over the sky for most of the year, the diffuse radiation is dominant on the window except from November to February.

For the slat window, the slats can be tilted to a different angle to intercept the beam radiation from entering the modeled room. Fig. 12(b) shows the percentage of time that the beam radiation is completely shaded by the slats. The percentage values are obtained

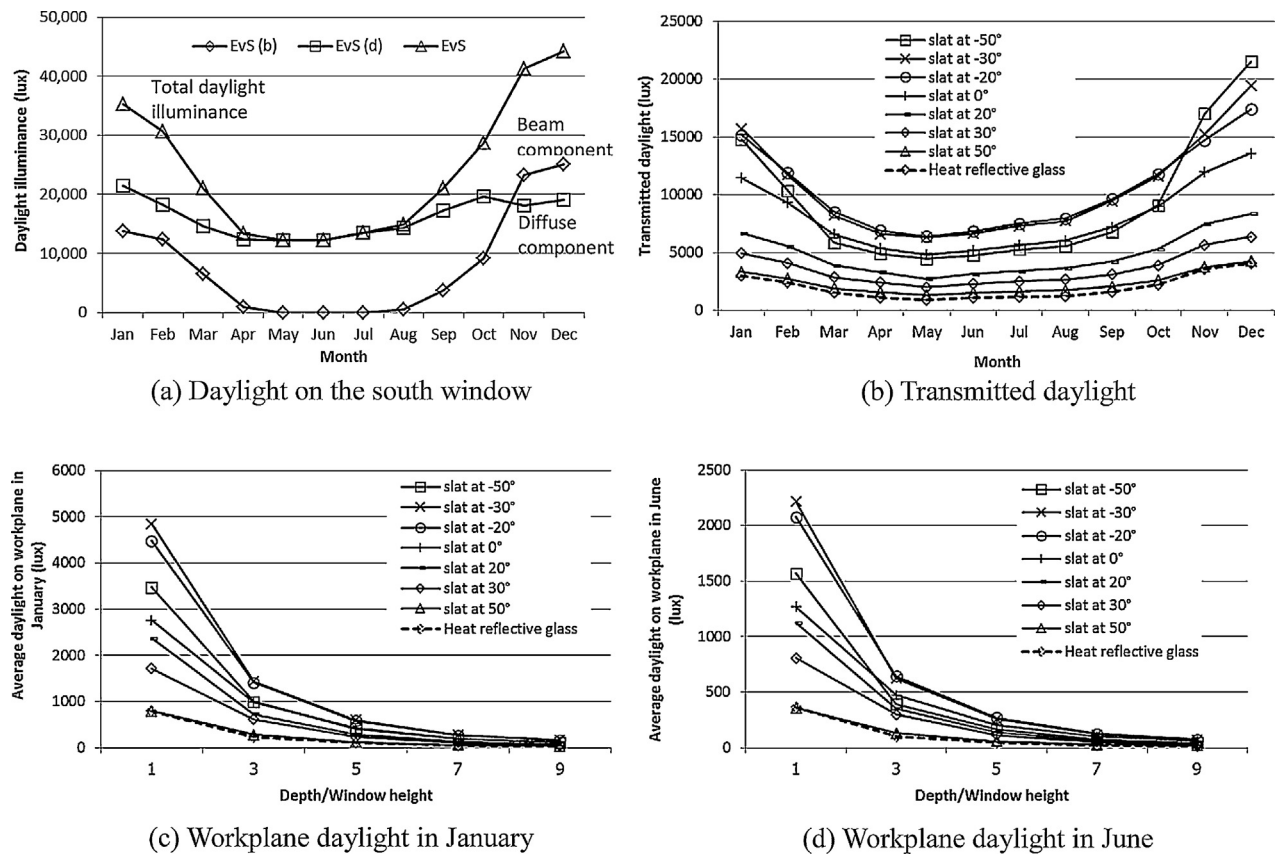


Fig. 13. Daylight simulations of the slat window facing south.

by dividing the number of calculations giving $F_b = 0$ with the total calculations made in the working hour period. In the figure, the plot is shown for the selected slat angles of -50° , -30° , -20° , 0° , 20° , 30° , and 50° . It is observed that at 0° (horizontal position), the beam radiation is fully shaded and cannot enter the room over the whole working period from March to September (The sun stays northern from May to August). In other months, the fully sun-shaded period decreases and is shortest in December but still more than 70% of the working hours. In the figure, it is essential to rotate the slats counterclockwise exceeding 30° to ensure no direct entering of the beam radiation throughout the year.

Fig. 12(b) also shows that rotating the slats clockwise from 0° (the slat angle in the negative range) sharply decreases the sun shading. None of the working hours during November–February, the slats at -50° can fully shade the beam radiation. For the glazed window with no shading device, the beam radiation enters the room for all times when the sun appears in front of the window. Fig. 12(c) shows the corresponding values of the ratio of the sun-shaded area to the window area ($1 - F_b$). From the figure, rotating the slats counterclockwise from -50° to 50° results the increasing sun-shaded area.

Fig. 12(d) shows the monthly average of the transmitted solar radiation from the slat window. It is obvious that the transmitted radiation is highly dependent on the slat angle. At 0° , the transmitted radiation is around 20 W/m^2 during April–August; approximately 20% of the incident radiation. Its value is highest at an average of 48 W/m^2 in December, but this amount is only 14% of the corresponding solar incidence. The slats can effectively shade the beam component.

Rotating the slats counterclockwise from 0° reduces the transmitted radiation. At these positions (slat angle), the slats intercept more of the incident radiation and reflect it to the exterior. At 30° ,

the transmitted radiation does not exceed 22 W/m^2 on average and is comparable to that of the heat reflective glass with 6% solar transmittance.

In general, rotating the slats clockwise from 0° tends to increase the transmitted radiation. The openings between the slats that direct to the sky allow more solar radiation penetration through the openings. The incident radiation on the upper slat surface is also reflected into the room interior. In the figure, the slats at -20° maximize the solar transmission from February to October. In November, December and January, the transmitted radiation is highest at the angle of -50° . Observing Fig. 12(c), the sun-shaded area at -50° is only 20% of the window area during the three months.

Fig. 12(e) shows the total thermal gain of the slat window. The gain comprises three parts of (i) the transmitted solar radiation (as shown in Fig. 12(d)), (ii) the inward heat flow due to the absorbed solar radiation and (iii) the heat transfer by the temperature differential between the ambient air and the room air. In most cases, the total thermal gain is largest at -20° , but it is comparable to that of the heat reflective glass. For our location where the latitude and longitude are 14.7°N and 100.5°E , in order to completely shade the beam radiation during the office hours, Fig. 12(b) shows that the slats are needed to be limited at 30° during November–February, at 10° in March and October, and at 0° from April to September. As the result of this shading, the slat window can reduce 17.2–32.7% of the total thermal gain of the heat reflective glass.

Fig. 12(f) shows the share of the transmitted solar radiation on the total thermal gain. As daylight presents the visible part of solar radiation, the higher the value of the share indicates the better the daylighting performance of the slat window in terms of increasing transmitted daylight flux per unit of the total heat gain. The plots in Fig. 12 indicate that the slat window has superior thermal per-

Table 6

The luminaire and lighting power density for interior lighting in the modeled room.

Light Luminaire				
Number of lamp	2			
Number of ballast	1			
Total light flux (lm)	5360.0			
Total power (W)	74.0			
Efficacy (lm/W)	72.4			
Workplane illuminance (lx)	800	500	300	
Light power density (W/m ²)	28.0	17.5	10.5	

formance to the heat reflective glass for an air-conditioned daylit room.

6.1.2. Daylight transmission

The results from the daylight simulation are next presented. Fig. 13(a) shows the monthly average value of the daylight illuminances on the south facing window. The value varies from 12 klx in May to 44 klx in December and in similar pattern with the solar incidence.

In Fig. 13(b), the transmitted daylight from the window is plotted against the slat angle. Influence of the slats on the daylight transmission is clearly observed. In most of the time, the transmitted daylight is highest at -20° . The sharp increase of the transmitted daylight at -50° in November-January is due to entering direct sunlight.

Fig. 13(c) shows the daylight illuminance on the workplane level in January (the sun is in front of the window). The workplane daylight is high near the windowed wall and reduces exponentially along the distance to the rear wall. The slats at -30° give the highest workplane daylight for all points in the room.

Fig. 13(d) shows the workplane daylight in June (the sun stays behind the window). Distinct from the previous (Fig. 13(c)), the slats at -20° give the highest workplane daylight except the area close to the windowed wall ($D/H_w = 1$). This pattern actually occurs for eight month from February to October.

Examining Fig. 13(c) and (d), the daylight from the slat window in the tropics is abundant for the interior illumination. By altering of the slats from -30° to 50° , the workplane daylight could be regulated from its maximum to minimum values. For the heat reflective glass, the workplane daylight illuminance is rather lower and comparable to that from the slat window at 50° (fully closed).

6.1.3. Energy performance

The above simulation results were next used to evaluate the energy consumptions of the interior lighting and air-conditioning of the modeled room. It was assumed that ceiling-mounted luminaires are used to provide the uniform workplane illuminance at 0.75 m above floor. Each luminaire is housed with two T8 fluorescent lamps (36 W each) and one electronic ballast (2 W). Table 6 summarizes the specific information of the luminaires and its rated power calculated using the IESNA Lumen method. From the table, to meet the target illuminance at 800, 500 and 300 lx, the lighting power densities (LPD) are at 28.0, 17.5 and 10.5 W/m², respectively.

With the daylighting, the dimming controller is used to regulate the light from electric lamps to supplement the daylight. The electric power is lowered linearly with the lighting reduction. However, the system still consumed electricity at 10% of its rated power even when the daylight alone could meet the target illumination level.

For the air-conditioning, the cooling load is defined as the total sum of the dissipated heat from the electric lamps and the total thermal load from the window. The calculations postulate that the electricity supplied to lamps is finally converted to heat. As such, the heat load from the lamps is also equal to LPD value. The thermal load from the slat window can be calculated by the thermal model.

$$E_w = (LLF) (CU) (L_f/P) (P/A)$$

where

$$\begin{aligned} E_w &= \text{Target workplane illuminance} \\ LLF &= \text{Light loss factor (assumed 0.8)} \\ CU &= \text{Coefficient of Utilization (assumed 0.5)} \\ L_f/P &= \text{Efficacy} \\ P/A &= \text{Light power density} \end{aligned}$$

The power requirement for the air-conditioning can be obtained by dividing the total cooling load with the air-conditioning system Coefficient of Performance (COP). Eq. (25) expresses the monthly energy consumption of the room with the slat window (En) in unit kWh/year:

$$En = \left(LPD + \frac{CL \cdot (A_w/A_f)}{COP} \right) \cdot A_f \cdot H, \quad (25)$$

where LPD is the average lighting power density of the lighting system (in unit W/m₂). CL is the total heat gain from the slat window (in unit W/m_w²). COP is coefficient of performance of the air-conditioning system and assumed equal to 2.7 in the study. H is the working hours in each month. A_w and A_f stand for the window area and the floor area of the modeled room, respectively. Eq. (25) is a reduced form of the energy equation of Thailand building energy code that are used to evaluate the energy consumption of a designated building in comparison with the reference building complying with the minimum energy performance requirements [6].

By using the simulated workplane daylight, the LPD_x to meet a target illuminance can be determined as a function of the distance from the windowed wall (x). Fig. 14(a) shows exemplarily the LPD_x to meet the target of 500 lx in January.

The LPD_x values of x at $D/H_w = 1$ are quite similar for all slat angles. The workplane daylight near the windowed wall is sufficient or even exceeding the target requirement. However, deep into the room (e.g. x at $D/H_w = 2$ upto 9), more electric light is required to supplement the daylight. The LPD_x values are thus increasing and distinct among the slat angles. In the figure, the LPD_x value of the non-dimmable uniform lighting is given for benchmarking.

The average LPD of the modeled room was derived from the LPD_x . The lighting energy consumption was calculated in sequence. Fig. 14(b) shows the monthly consumption of the electric lighting. It is observed that the consumption varies from month to month. The consumption is lowest at -20° , since the daylight from the window is maximized.

Fig. 14(c) shows the air-conditioning energy consumption. The consumption is quite comparable for all angles except at 50° . The larger thermal gain from introducing more daylight can be counterbalanced by the reduced heat from the dimmed lamps. In all cases, the room with the slat window consumes less air-conditioning energy than the same room using heat reflective glazing window. This result assures no thermal penalty from the daylighting from the slat window couple with the dimmable electric lighting.

In Fig. 14(d), the annual energy consumptions of the modeled room is minimum at the angle of -20° . It should be noted that the results in the figure assume the slats are fixed at an angle throughout the year. The analysis considered only in the energy aspect with no concern of human comfort.

To further our study, a daylighting scheme was introduced for which the slats would be altered to minimize the room energy consumption without the direct entering of beam radiation. Under this scheme, it is expected that the occupants near the window would less experience with thermal discomfort and visual glare. Fig. 15

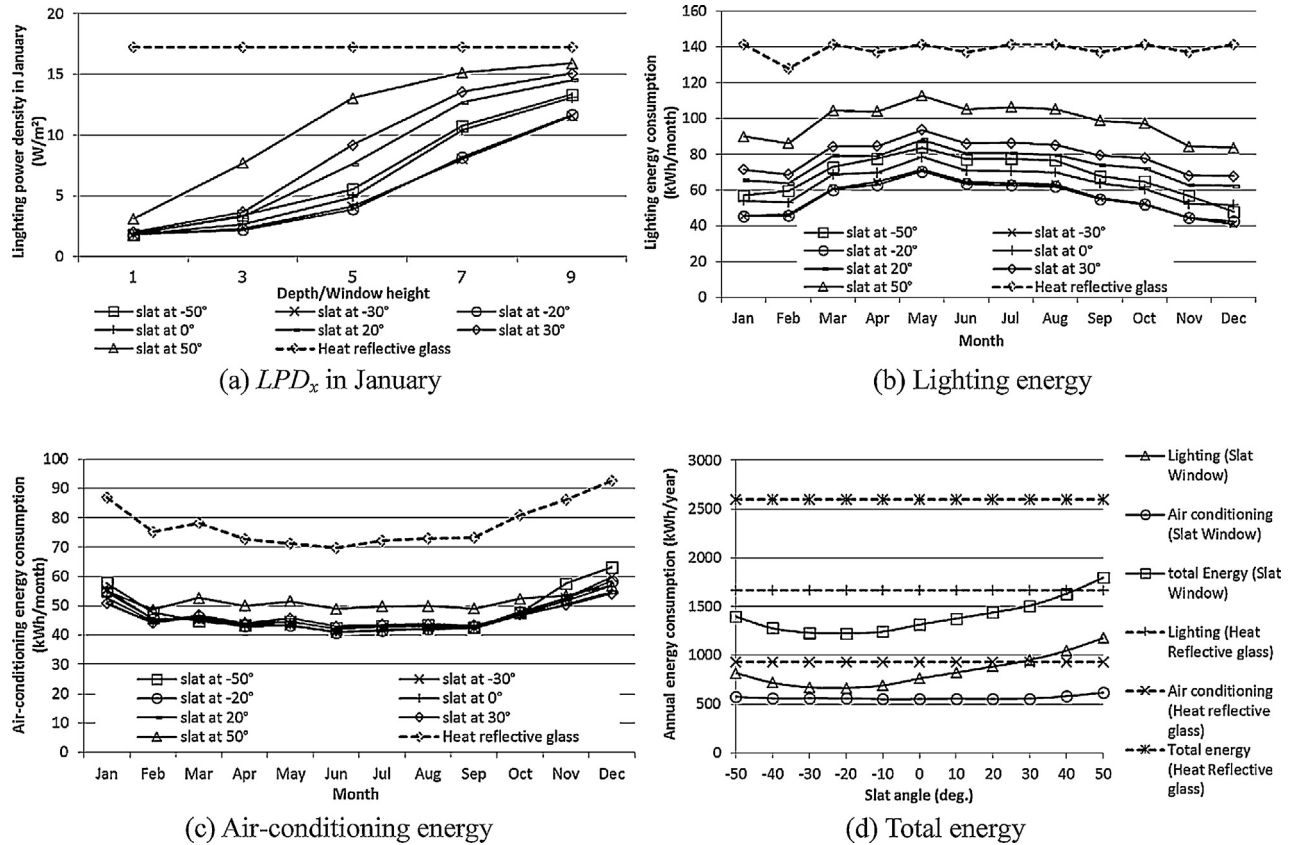


Fig. 14. Energy calculations of the room with the slat window facing south (The target illuminance of 500 lx).

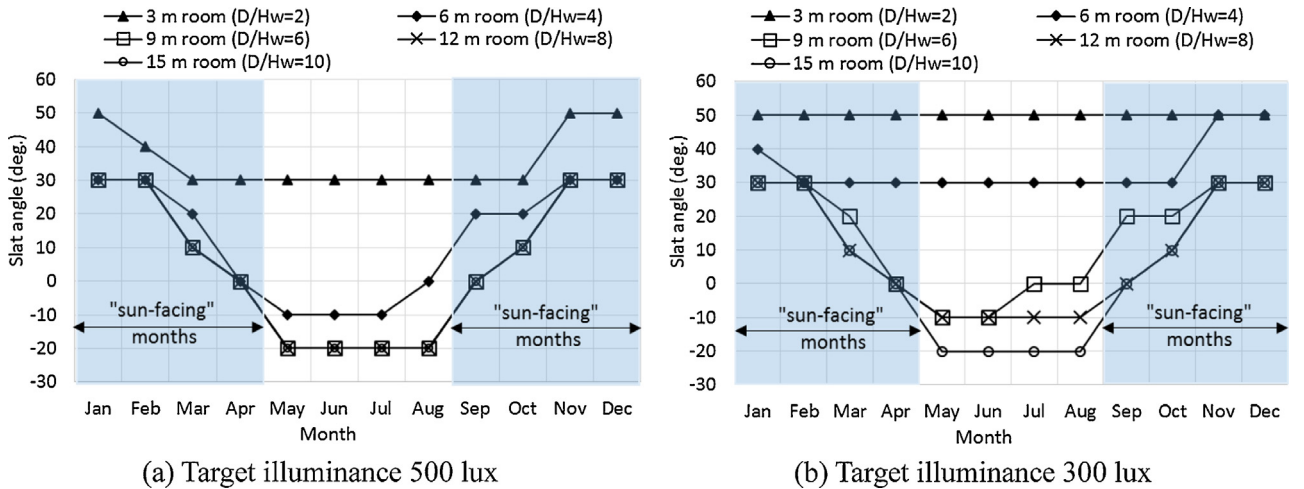


Fig. 15. The slat position of a daylight scheme to minimize energy consumption of the modeled rooms and to prevent the beam radiation entering.

shows the slat positions (angle) that correspond with the lowest monthly energy consumption of the rooms with 3 m, 6 m, 9 m, 12 m and 15 m depths. The shaded area in the plots presents the months that the sun is in front of the window (the "sun-facing" months) and the slat angle is needed to be limited to prevent the beam radiation entering.

Examining Fig. 15(a) where the target workplane illuminance is 500 lx, for the room with its depth more than four times of the window height ($D/H_w > 4$, room depth > 6 m), the daylight from the window are to be maximized for the lowest energy consumption. The slats are to be set at the limited angle that prevents the beam radiation entering in the "sun-facing" months. In the remaining

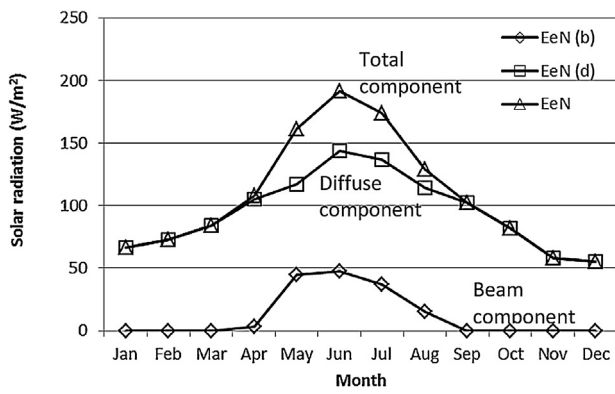
months, the slats are set at -20° to introduce more daylight to minimize the energy consumption.

This practice could also be applied for the room requiring higher workplane illuminance (exceeding 500 lx). For the lower illuminance target (e.g. 300 lx), the slats are to be tilted to reduce the transmitted daylight and avoid excessive solar gain as shown in Fig. 15(b). Table 7 summarizes the annual energy consumption of the room with the slats set according to the position in Fig. 15. The consumption of the modeled office room with heat reflective glass is given for benchmarking. It can be observed that significant energy savings of 41.6–71.8% can be achieved by this simple daylighting scheme.

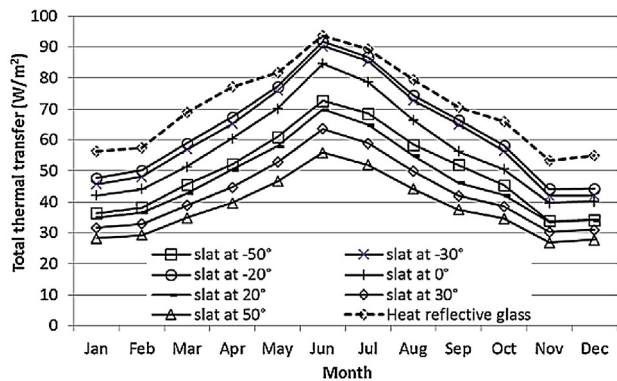
Table 7

The energy consumptions of the room with slat window facing south.

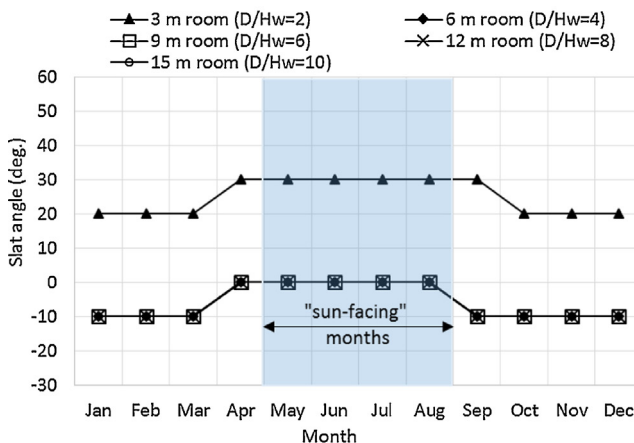
Room depth (m)	Target illuminance (lx)	Annual energy consumption (kWh/year)						Energy savings (%)		
		Room with the slat window			Room with the heat reflective glass window			Light	Air-con	Total
		Light	Air-con	Total	Light	Air-con	Total			
3	300	44.8	191.8	236.5	199.9	389.6	589.5	77.6	50.8	59.9
	500	50.3	209.3	259.6	333.2	438.9	772.1	84.9	52.3	66.4
	800	58.4	236.7	295.1	533.1	513.0	1046.1	89.0	53.9	71.8
6	300	86.6	227.5	314.1	399.8	463.6	863.4	78.3	50.9	63.6
	500	106.4	272.6	379.0	666.3	562.4	1228.7	84.0	51.5	69.2
	800	205.3	322.9	528.2	1066.1	710.5	1776.6	80.7	54.6	70.3
9	300	140.5	284.9	425.4	588.8	533.6	1122.4	76.1	46.6	62.1
	500	261.0	343.5	604.5	981.3	679.0	1660.3	73.4	49.4	63.6
	800	558.9	453.9	1012.8	1570.1	897.1	2467.2	64.4	49.4	58.9
12	300	233.7	357.0	590.6	799.6	611.7	1411.3	70.8	41.6	58.2
	500	521.2	439.9	961.1	1332.7	809.1	2141.8	60.9	45.6	55.1
	800	1024.4	626.3	1650.7	2132.3	1105.3	3237.6	52.0	43.3	49.0
15	300	340.4	433.9	774.2	999.5	685.7	1685.2	65.9	36.7	54.1
	500	807.8	546.1	1353.8	1665.8	932.6	2598.4	51.5	41.4	47.9
	800	1510.8	806.4	2317.2	2665.3	1302.8	3968.1	43.3	38.1	41.6



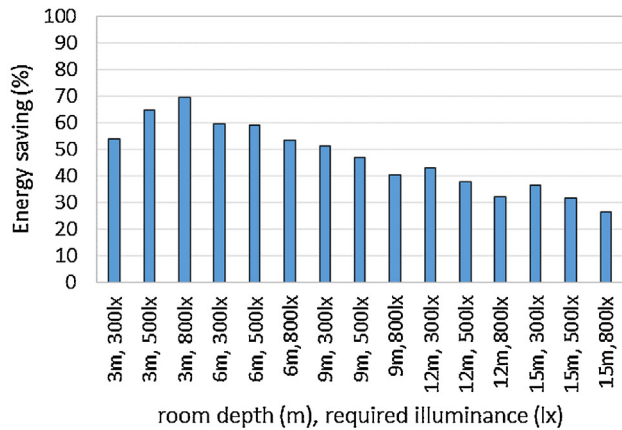
(a) Incident solar radiations



(b) Total thermal gain



(c) Optimum slat position for 500 lux



(d) Energy savings

6.2. The north facing slat window

The simulations were performed for the north-facing slat window. Fig. 16(a) shows that the incident solar radiations on the window are relatively low and the beam component shares a minor portion in the total solar incidence. As a result, the total thermal gain is lower compared to that of the south-facing slat window

(Fig. 16(b)). Not given in the figure, the daylights on the window vary with the similar patterns to the incident solar radiations. The average peak illuminance value is 22 klx in June.

In Fig. 16(c), the slat angles that minimize the energy consumption for the target illuminance of 500 lx are presented. As the solar elevation is high throughout the office hours during the "sun-facing" months (May–August), the slats can be fully opened (at 0°)

Fig. 16. Thermal and daylight simulations of the slat window facing north.

to introduce the diffuse daylight. Compared to the heat reflective glass, the energy savings can be achieved in a range of 25–70% from the slat window (Fig. 16(d)). These savings are marginally smaller in percentage term than those of the south-facing slat window.

7. Conclusion

This paper investigated the energy performance of the daylighting from the slat window under tropical climate. In the study, a non-steady state thermal model was developed for the short-time step thermal simulation of the slat window. The model analysis was based on the radiative exchanges and heat convections among the window components and accounted for the thermal storage effect in the system energy balance. From the experimental validation, the model could well predict the transmitted solar radiation and the surface temperatures of the window components under varying solar radiation and ambient conditions.

In the simulation study, the thermal performance of the slat window was evaluated by using the validated thermal model. In our tropical region where the solar elevation is high, the solar radiation and daylight on the south and the north windows are dominant by the sky diffuse component for most daytime. The incident beam radiation can be fully shaded by the slats with shallow tilted angles during the office hours. In comparison with the heat reflective glass window, the slat window reduces 17.2–32.5% of the total thermal gain when the beam radiation can be fully shaded.

The daylight model developed in our previous works was used to determine the daylight from the slat window. The tradeoff between the total thermal gain and the transmitted daylight was demonstrated by evaluating the lighting and air-conditioning energy consumption of the modeled room using the modified energy equation of the Thai building energy code. The slat angles that minimize the energy consumption in each calendar month without the beam radiation entering were determined as functions of the room depth to window height ratio and the target workplane illuminance. The results show that for the room with its depth greater than four times of the window height and the target workplane illuminance higher than 500 lx, the slat angle should be set to maximize the daylight transmission. However, the slat position is limited at the angles to prevent the beam radiation entering in the “sun-facing” months. For the shallower room and lower target illuminance, the slats are needed to intercept more solar radiation to avoid excessive solar heat gain. With this simple passive slat control, the energy consumption of the room with the slat window can be saved 25–70% compared to that of the same room using the heat reflective glass.

In this simulation, the presumptions of the modeled room were the perfectly diffusive surfaces for both solar radiation and daylight. The reflectances of the ceiling, walls, and floor were 0.7, 0.5, and 0.3, respectively. The outdoor ground reflectance was assumed at 0.05. The room occupation was from 8:00–17:00. The lighting equipment was ceiling mounted T8 fluorescent lamp with electronic ballast. The occupants sitting close to the window do not have thermal discomfort and visual glare. No thermal penalty from the daylighting from the slat window couple with the dimmable electric lighting. The slats were introduced for the window facing south and north.

In Thailand, building energy code was promulgated to enforce the designated buildings to comply with the minimum energy performance requirements. The code was strengthened and daylighting has been promoted through the code since 2011. By using the developed thermal and daylight models together with the energy equation of the code, the calculated energy consumption reduction from the use of the slat window can be applied for the daylighting accreditation. In the model implementation, the parameters in the presumption can be assigned with other appropriate values according to considered room configurations.

Nowadays, as computerized systems for energy management are implemented more widely in medium and large commercial buildings, for a further study, an automated system of the slat window will be investigated for energy conservation potential with consideration of the occupant thermal and visual comforts.

Acknowledgement

The financial support from the National Science and Technology Development Agency (NSTDA), grant no. P-12-01728 through this research project is gratefully acknowledged.

References

- [1] I.R. Edmonds, P.J. Greenup, Daylighting in the tropics, *Sol. Energy* 73 (2) (2002) 111–121.
- [2] S. Chirarattananon, P. Chaiwiwatworakul, S. Pattanaseethanon, Daylight availability and models for global and diffuse horizontal illuminance and irradiance for Bangkok, *Renew. Energy* 26 (1) (2002) 69–89.
- [3] S. Chirarattananon, P. Chaiwiwatworakul, Distributions of sky luminance and radiance of north Bangkok under standard distributions, *Renew. Energy* 26 (8) (2007) 1328–1345.
- [4] P. Chaiwiwatworakul, S. Chirarattananon, P. Rakwamsuk, Application of automated blind for daylighting in tropical region, *Energy Convers. Manage.* 50 (12) (2009) 2927–2943.
- [5] P. Chaiwiwatworakul, S. Chirarattananon, A double-pane window with enclosed horizontal slats for daylighting in buildings in the tropics, *Energy Build.* 62 (2013) 27–36.
- [6] S. Chirarattananon, P. Chaiwiwatworakul, V.D. Hien, P. Rakwamsuk, K. Kubaha, Assessment of energy savings from the revised building energy code of Thailand, *Energy* 35 (4) (2010) 1741–1753.
- [7] S. Rheault, E. Bilgen, Heat transfer analysis in an automated venetian blind window system, *J. Sol. Energy Eng.* 111 (1989) 89–95.
- [8] S. Rheault, E. Bilgen, Experimental study of full-size automated venetian blind window, *Sol. Energy* 44 (3) (1990) 157–160.
- [9] S. Chaiyapinunt, S. Worasinchai, Development of a model for calculating the longwave optical properties and surface temperature of a curved venetian blind, *Sol. Energy* 83 (2009) 817–831.
- [10] S. Chaiyapinunt, S. Worasinchai, Development of a mathematical model for a curved slat venetian blind with thickness, *Sol. Energy* 83 (2009) 1093–1113.
- [11] T.E. Kuhn, Solar control: a general evaluation method for facades with venetian blinds or other solar control systems, *Energy Build.* 38 (6) (2006) 648–660.
- [12] T.E. Kuhn, Solar control: comparison of two new systems with the state of the art on the basis of a new general evaluation method for facades with venetian blinds or other solar control systems, *Energy Build.* 38 (6) (2006) 661–672.
- [13] D. Alessandro, T.E. Kuhn, L. Pagliano, Modelling the solar factor of glazing combined with indoor venetian blinds, in: PLEA2006—The 23rd Conference on Passive and Low Energy Architecture, Geneva, Switzerland, 6–8 September, 2006.
- [14] F. Zanghirella, M. Perino, V. Serra, A numerical model to evaluate the thermal behaviour of active transparent façades, *Energy Build.* 43 (2011) 1123–1138.
- [15] E.S. Lee, D.L. DiBartolomeo, S.E. Selkowitz, Thermal and daylighting performance of an automated venetian blind and lighting system in a full-scale private office, *Energy Build.* 29 (1) (1998) 47–63.
- [16] M.H. Oh, K.H. Lee, J.H. Yoon, Automated control strategies of inside slat-type blind considering visual comfort and building energy performance, *Energy Build.* 55 (2012) 728–737.
- [17] EnergyPlus, Engineering Document: The Reference to Energyplus Calculations, US Department of Energy, 2013.
- [18] F. Hammada, B. Abu-Hijleh, The energy savings potential of using dynamic external louvers in an office building, *Energy Build.* 42 (10) (2010) 1888–1895.
- [19] G. Rapone, O. Saro, Optimisation of curtain wall facades for office buildings by means of PSO algorithm, *Energy Build.* 45 (2012) 189–196.
- [20] P. Correia da Silva, V. Leal, M. Andersen, Influence of shading control patterns on the energy assessment of office spaces, *Energy Build.* 50 (2012) 35–48.
- [21] H.H. Alzoubi, A.H. Al-Zoubi, Assessment of building facade performance in terms of daylighting and the associated energy consumption in architectural spaces: vertical and horizontal shading devices for southern exposure facades, *Energy Convers. Manage.* 51 (8) (2010) 1592–1599.
- [22] P. Chaiwiwatworakul, S. Chirarattananon, Evaluation of sky luminance and radiance models using data of north Bangkok, *LEUKOS* 1 (2) (2004) 177–197.
- [23] E.U. Finlayson, D.K. Arastech, C. Huizinga, M.D. Rubin, M.S. Reilly, Window 4.0: Documentation of Calculation Procedures. Publication LBL-33943/UC-350, Lawrence Berkeley Laboratory, Energy & Environmental Division, Berkeley, CA, 2008.
- [24] ASHRAE, ASHRAE Handbook-1985 Fundamentals, American Society of Heating, Refrigerating and Air-Conditioning Engineers, Inc., Atlanta, 1985.
- [25] M. Collins, S. Tasnim, J. Wright, Determination of convective heat transfer for fenestration with between-the-glass louvered shades, *Int. J. Heat Mass Transfer* 51 (2008) 2742–2751.

- [26] S.H. Cho, K.S. Shin, M. Zaheer-uddin, The effect of slat angle of windows with venetian blinds on heating and cooling loads of buildings in South Korea, *Energy* 20 (12) (1995) 1225–1236.
- [27] X.L. Xu, Z. Yang, Natural ventilation in the double skin facade with venetian blind, *Energy Build.* 40 (8) (2008) 1498–1504.
- [28] H. Manz, Total solar energy transmittance of glass double façades with free convection, *Energy Build.* 36 (2) (2004) 127–136.
- [29] A. Nabil, J. Mardaljevic, Useful daylight illuminances: a replacement for daylight factors, *Energy Build.* 38 (7) (2006) 905–913.
- [30] IES, Committee on Calculation Procedures IES Recommended Practice for the Lumen Method of Daylight Calculations. IES RP-23-1989, Illuminating Engineering Society, New York, 1989.